Sedimentary Geology 408 (2020) 105730

Contents lists available at ScienceDirect

Sedimentary Geology

journal homepage: www.elsevier.com/locate/sedgeo

Mixed siliciclastic-carbonate-evaporite sedimentation in an arid eolian landscape: The Khor Al Adaid tide-dominated coastal embayment, Qatar

John M. Rivers [a,*], Robert W. Dalrymple [b], Ruqaiya Yousif [b], Ismail Al-Shaikh [a], Josh D. Butler [a], Christopher Warren [c], Sabrina L. Skeat [a,1], Ekhlas M.M. Abdel Bari [d]

[a] Qatar Center for Coastal Research, ExxonMobil Research Qatar, Doha, Qatar
[b] Queen's University, Department of Geological Sciences and Geological Engineering, Kingston, Ontario, Canada
[c] ExxonMobil Canada, St. John's, Newfoundland, Canada
[d] Qatar University Environmental Science Center, Doha, Qatar

ARTICLE INFO

Article history:
Received 6 April 2020
Received in revised form 20 July 2020
Accepted 21 July 2020
Available online 28 July 2020

Editor: Dr. Brian Jones

Keywords:
Arid
Eolian
Marine
Lagoon
Evaporite
Qatar

ABSTRACT

The Khor Al Adaid embayment of southern Qatar represents a unique shallow-water mixed siliciclastic-carbonate coastal depositional system that developed in a hyper-arid climatic setting over the past 6000 years. The embayment, which was formed during the Flandrian transgression as a result of flooding across a partially fault-controlled incised fluvial drainage, is supplied by quartz-rich sands delivered by wind-blown dunes migrating southward across the surface of Qatar. These offshore-migrating eolian-derived sediments are being redistributed by tidal currents in an otherwise low-energy coastal zone, where in situ formation of carbonate mud and a low-diversity skeletal assemblage is ongoing within salinity-restricted environments. Three depositional sectors are delineated: 1) an energetic, linear, fault-controlled Entrance Channel into which the eolian dunes spill directly; 2) a relatively deep (up to 20 m) Outer Lagoon, interpreted to represent a flooded karst-collapse structure; and 3) a sprawling, low-energy, shallow (<2 m) Inner Lagoon occupying low-lying areas between deflated eolian dunes.

Physical oceanographic modeling, integrating multi-seasonal current meter and tidal gage measurements, demonstrates tidal current flow velocities are relatively high in both the Entrance Channel and at the constricted entrance to the Inner Lagoon. Associated flow expansion into less confined areas results in deposition of the eolian-derived sands as flood-tidal deltas, one in the Outer, and two in the Inner Lagoon. A weakly-developed ebb-tidal delta occurs where the Entrance Channel debouches into the Arabian Gulf. Flood-tide dominance is also apparent in Entrance Channel deposits, where sand accumulates in seaward-terminating "ebb barbs" along the margins of the flood-dominant thalweg. Such flood-tide dominance of the thalweg is unusual and likely reflects the absence of river discharge. Evidence of significant inverse estuarine circulation (seaward flow of a brine along the embayment floor) is mostly absent in spite of the landward increase of salinity, where concentrations reach more than double normal seawater salinity in the Inner Lagoon. Modeling results show that seaward-flowing brines formed in the Inner Lagoon are trapped in the relatively deep Outer Lagoon, and that mixing by tidal currents in the energetic Entrance Channel precludes the formation of vertical density gradients there. Because siliciclastic mud is essentially absent, and most of the sediment forming the deltas consists of sand, upper intertidal deltaic deposits that would normally consist of mud are absent, resulting in the flood-tide deltas having a pronounced lobate geometry similar to that of fluvial deltas formed predominantly of sand.

Away from tidal deltas, low-energy lagoons are floored by carbonate mud of local production, with minor gypsum precipitating in the Inner Lagoon. Wind-generated waves only locally influence sedimentation, forming complex nearshore bars along some lagoonal shorelines. The overall landward increase in salinity is accompanied by a decrease in the diversity of benthic fauna and their skeletal remains. A fairly diverse faunal assemblage is observed in the Entrance Channel near the Arabian Gulf, including colonial corals, whereas the inner lagoon assemblage is dominated gastropods belonging to *Pirenella cingulata*. The remnants of large eolian dunes are preserved in the low-energy setting of the Inner Lagoon, segmenting the waterbody, and locally increasing restriction. The sedimentology of the arid-zone coastal Khor Al Adaid embayment may serve as an analogue for environmental settings that were perhaps more commonplace in arid zones of flooded continents during greenhouse times.

* Corresponding author at: ExxonMobil Research Qatar, P.O. Box 22500, Qatar Science & Technology Park-Tech 2, Doha, Qatar.
E-mail address: John.m.rivers@exxonmobil.com (J.M. Rivers).
[1] Contractor.

https://doi.org/10.1016/j.sedgeo.2020.105730

1. Introduction

One of the recurring themes in published studies of eolian deposits is the transition between sandy deserts (ergs) and adjacent fluvial or marine environments. Ancient erg-margin successions where eolian sands interfinger with marine coastal deposits have been the subject of many studies, with examples documented from the Pennsylvanian-Permian of Utah and Wyoming (Huntoon and Chan, 1987; Kamola and Chan, 1988; Kerr and Dott Jr, 1988; Chan, 1989; Kamola and Huntoon, 1994; Ciftci et al., 2004; Jordan and Mountney, 2010, 2012; Blanchard et al., 2016), the Permian North Sea (Glennie and Buller, 1983), the Jurassic of Utah (Eschner and Kocurek, 1988; Jones and Blakey, 1993; Blakey et al., 1996; Mariño and Morris, 1996), the Cretaceous of Spain (Rodríguez-López et al., 2008, 2012), the Pleistocene of offshore Mauritania (Hanebuth et al., 2013), and the Holocene of the Persian Gulf (Shinn, 1973; Doornkamp et al., 1980; Fryberger et al., 1983). The earlier studies focus on a detailed reconstruction of the eolian bedforms, and particularly on the development and preservation of paleotopographic relief on the top of the eolian deposits. More recent studies (Rodríguez-López et al., 2008, 2012; Blanchard et al., 2016) examine the interbedded marine deposits in more detail, but are hampered in their analyses by the scarcity of comprehensive descriptions of the very few modern analogues that exist (e.g., northern Mauritania– Sarnthein and Walger, 1974; Sarnthein and Diester-Haass, 1977; Barusseau et al., 2010); Baja California, Mexico (Fryberger et al., 1990); and the southwestern coast of the Arabian Gulf (i.e., Saudi Arabia, Qatar and United Arab Emirates; Purser and Evans, 1973; Shinn, 1973; Fryberger et al., 1983; Lokier et al., 2013; Billeaud et al., 2014). Thus, additional studies of modern arid-zone coastal environments are needed. This is especially the case for areas where coastal transgression is occurring in a setting where the eolian dunes are migrating in an offshore direction, because this is likely to generate a more complex stratigraphic organization than in cases where the wind blows onshore (cf. Fryberger et al., 1983). One of the key modern analogues that has been used to interpret the interfingering of eolian and marine deposits is the Khor Al Adaid (a.k.a. the "Inland Sea", also abbreviated as the KAD) of southeastern Qatar (Rodríguez-López et al., 2012; Blanchard et al., 2016).

The Khor Al Adaid, an embayment with an area of 150 km^2 that separates Qatar from the Kingdom of Saudi Arabia to the south, lies along the southern margin of the Arabian Gulf (Fig. 1), which is a shallow, warm-water, evaporative marine system well known for its production of photozoan carbonates (Purser and Loreau, 1973). The waters bathing the coasts in this arid setting are subject to significant seasonal temperature fluctuations, as well as elevated salinities due to high evaporation rates (Rivers et al., 2019a). Most of the highly-restricted "Inland Sea water body" (Clarke and Keij, 1973) is less than 5 m deep. Seafloor sediments include significant quantities of siliciclastic sands sourced from adjacent eolian dunes, and lesser quantities of skeletal grains that were generated in situ (mostly molluscs) (Purser and Evans, 1973; Al-Khayat and Al-Mohannadi, 2006), and minor ooids (Loreau and Purser, 1973). In more landward portions of the system carbonate muds are common, subtidal gypsum precipitation occurs (Loreau and Purser, 1973), and microbial-mat production is prolific in intertidal regions (Paulo and Dittrich, 2013). On a global scale, extensive shallow-water, highly evaporitic marine embayments like the Khor Al Adaid, which lacks fluvial input, are not common. However, during greenhouse times, when continents were flooded by epeiric seas, embayments of this type may have been commonplace, particularly in the desert latitudes. The purpose of this report is to document the geomorphology and facies of this complex marine embayment, and discuss the role that the arid setting and eolian processes play in determining its sedimentary characteristics. We hope that these observations will make this area a more useful analogue for shallow evaporative coastal systems in the rock record, and will provoke more interest and work on similar systems.

2. Setting and previous research

2.1. Geological and geomorphological setting

The Arabian Gulf is a foreland basin that formed as a result of ongoing collision between the Arabian and Eurasian plates, causing uplift of the Zagros mountain range in Iran (Stern and Johnson, 2010). Simultaneous uplift of the Qatar Arch has generated the Qatar peninsula, approximately 190 km in length (north-south) and 90 km in width, that protrudes northward into the southern Arabian Gulf (Fig. 1). Surface rocks of Qatar are predominantly Eocene-age limestones and dolostones of the Dammam and Rus formations (Seltrust, 1980). Pleistocene and Holocene carbonate rocks and sediments are mostly found in coastal regions, and clastic (quartz-rich) eolian sands are present mostly in the southeastern part of the country.

The shorelines of Qatar are a westward extension of the "Trucial Coast" (Purser and Loreau, 1973), where photozoan carbonates are currently being produced in a shallow, evaporative, ramp setting. Toward the Khor Al Adaid, the eastern coastal environments of Qatar include sabkhas and tidal flats, fronted by land-attached beaches or spits that are prograding to the south (Shinn, 1973; Billeaud et al., 2014). These give way seaward to mollusc-rich open-marine subtidal sediments (Purser and Evans, 1973; Wagner and van der Togt, 1973). Coral reefs are also found forming isolated banks along the eastern Qatar coastline (Purser and Evans, 1973), where ooid deposits have also been identified (Loreau and Purser, 1973). However, unlike much of the Trucial Coast where the winds blow onshore, winds along the eastern coast of Qatar blow offshore. In southeastern Qatar quartz-rich eolian dunes migrate toward the shoreline. As a result, the coastal deposits there consist mainly of siliciclastic sand, with a lesser component of carbonate shell material.

The coastal regions of Qatar have been significantly influenced by recent sea-level changes (Billeaud et al., 2014; Strohmenger and Jameson, 2015; Rivers et al., 2019b). Sea-level was approximately 120 m lower than today about 18,000 years ago (Fairbridge, 1961; Sarnthein, 1972; Kassler, 1973; Lambeck, 1996), during which time the entire Arabian Gulf was exposed. Approximately 14,000 years ago the Arabian Gulf flooded (Lambeck, 1996), and sea-level rose to the post-glacial highstand about 6000–7000 years ago, sea level at this time reaching about 1.5 to 4 m above the present-day level (Kassler, 1973; Lambeck, 1996; Engel and Brückner, 2014; Lokier et al., 2013; Rivers et al., 2019b) (Fig. 2). Since then sea level has fallen, reaching its present-day position approximately 1500 years ago based on regional and local studies (Lokier et al., 2013; Rivers et al., 2019b). The late Holocene sea-level fall is interpreted to be the result of global seawater redistribution associated with the effects of ice and meltwater loading (Mitrovica and Milne, 2002). Raised shoreline deposits (i.e., beach ridges) are present at various locations around the outer part of the Khor Al Adaid.

The eolian dunes of Qatar are concentrated in the southeastern portion of the county (Embabi and Ashour, 1993), in a belt that is 5–7 km wide parallel to the coast (Figs. 3, 4); the remainder of the land area consists of bedrock outcrops mantled by a thin, patchy veneer of sand, with localized accumulations of finer sediment in depressions, many of which are karstic in origin (Ashour, 1987; Engel et al., 2020). The dunes are composed mainly of fine to medium sand (Embabi and Ashour, 1993), with an admixture of coarse sand. The sand consists predominantly of quartz and is believed by most workers to have been derived from northern Saudi Arabia (Embabi and Ashour, 1993), although more recent compositional studies suggest that the source might be from the Zagros Mountains and Tigris-Euphrates River in Iran, with the sand having been blown southward across the northern portion of the Arabian Gulf during the late Pleistocene sea-level lowstand (Garzanti et al., 2013). Since the sea-level rise, this source of sand has been cut off, and the dunes have migrated across the Qatar peninsula to its eastern coast where they are actively dumping sand into the sea (Fig. 4; Shinn, 1973; Rodríguez-López et al., 2012). Present-day

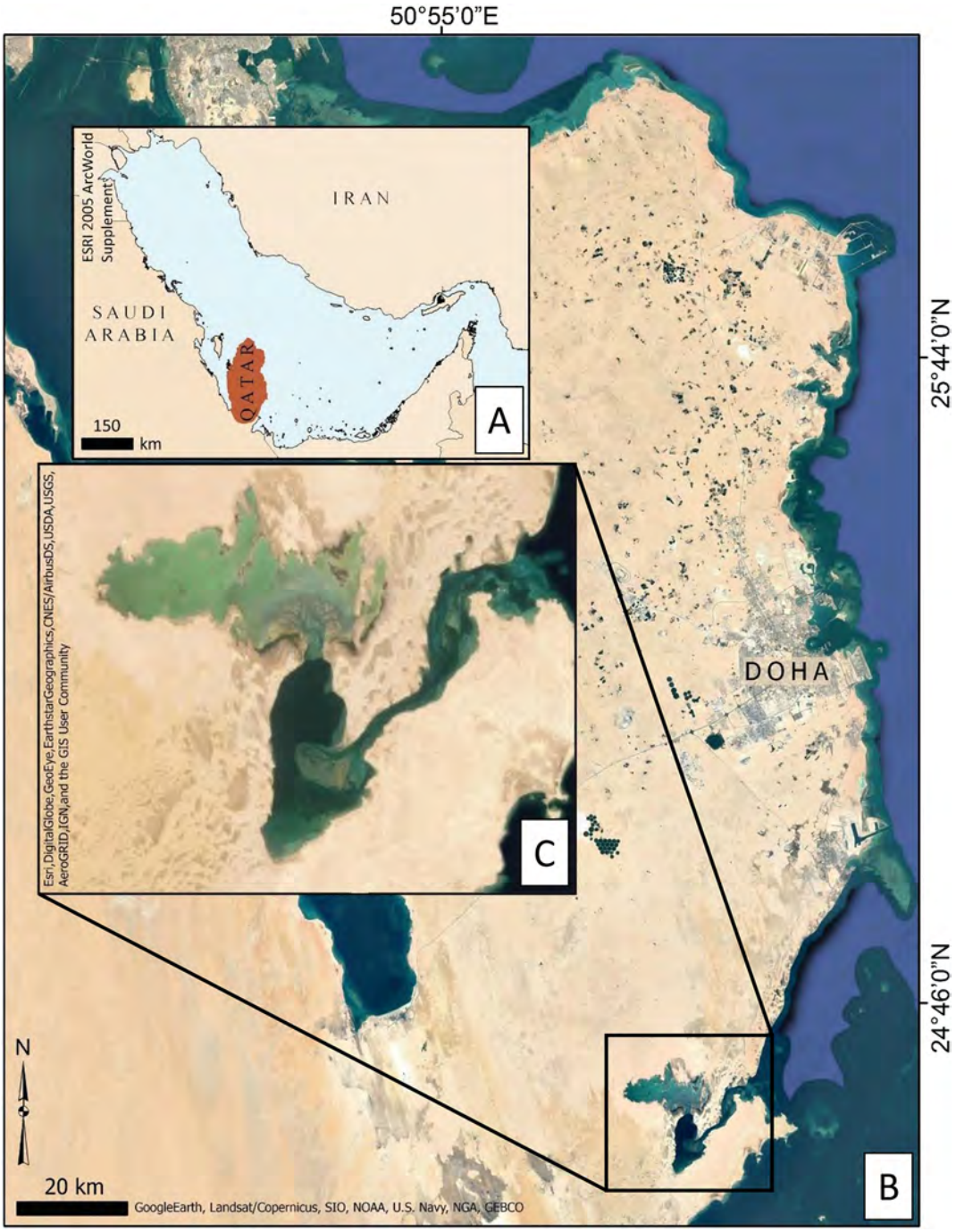

Fig. 1. (A) Map of the Arabian Gulf showing the location of Qatar (brown outline), which lies on the crest of the Qatar Arch, a deep-seated structure that is oblique to the trend of the foreland basin that the Gulf occupies. (B) Satellite image of western and southern Qatar, showing the location of the Khor Al Adaid. (C) Satellite image of the Khor Al Adaid. (For interpretation of the references to colour in this figure legend, the reader is referred to the web version of this article.)

migration rates are of the order of 10 m/a, with smaller dunes generally migrating more rapidly than larger ones (Embabi and Ashour, 1993). The dunes themselves range from 1 to 40 m high, with the majority being <10 m in height (Embabi and Ashour, 1993). Simple dunes are typically barchanoid in shape (Embabi and Ashour, 1993), although more linear forms are also present. Large linear dune ridges (draa) with spacings of 650–1500 m also occur. In the southeastern part of the dune field, these ridges are oriented NE-SW, but to the west they are oriented more NNE-SSW. All dunes rest on a nearly planar deflation surface (i.e., a super surface or Stokes surface; Stokes, 1968; Kocurek, 1988) that is occupied by coastal and inland sabkhas.

Southeastern Qatar hosts the evaporative Khor Al Adaid (Fig. 3), a tide-dominated estuary partly confined by bedrock. This marine embayment can be segregated into three distinct sectors: 1) an irregularly shaped "Inner Lagoon", referred to locally as the "Inland Sea", that is 73.5 km^2 in extent; 2) a somewhat smaller, elliptical "Outer Lagoon" with an aerial extent of 53.5 km^2, which is separated from the Inner Lagoon by a sandy ridge of possible dune origin; and 3) a narrow "Entrance Channel" that is less than 3 km in width and approximately 15 km in length connecting the Outer Lagoon to the open Arabian Gulf. Miocene strata (Dam Formation) are exposed along the southern shoreline of the channel (Fig. 3). Prominent 500-m-scale arcuate features

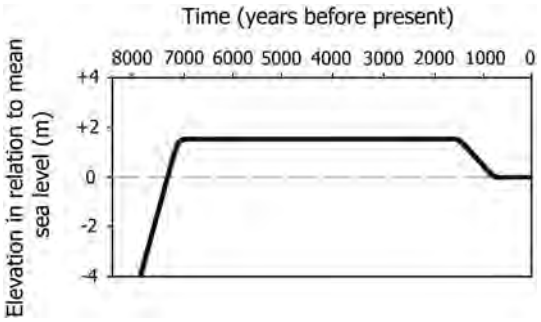

Fig. 2. History of sea level in Qatar and adjoining areas over the last 8000 years. About 7000 yrs. BP, sea level reached a highstand approximately 1.5 m above present-day sea level that persisted until about 1400 yrs. BP when it then fell to its present elevation. Based on various sources including Kassler (1973), Lambeck (1996), Engel and Brückner (2014), Lokier et al. (2013), and Rivers et al. (2019b).

observed along the southern channel bank near its entrance to the Outer Lagoon are interpreted as relict fluvial meanders, indicating this marine system occupies an incised drainage that was at least periodically active during sea-level lowstands. Flood-tidal deltas are observed in the system both where the channel connects to the Outer Lagoon, as well as at the mouth of the Inland Sea, propagating north from its Outer Lagoon connection. The Inner Lagoon is flanked to the north and west by exposed Eocene bedrock (Dammam Formation; Fig. 3). The entire Khor Al Adaid system is surrounded on its north, east and west sides by the active dune fields described above; the fewest number of active dunes lie to the north of the Inner Lagoon.

2.2. Climate and oceanography

The climate of Qatar is arid to hyper-arid (Eccleston et al., 1981; Glennie, 2005). Average precipitation in Doha is 7.7 cm/yr, with most precipitation occurring between November and April (Al Mamoon et al., 2014). Rainfall is not observed to influence salinity values of the Khor AL Adaid (Rivers et al., 2019a). Surface air temperature, humidity, and wind speed for southern Qatar, as well as water temperature for open southern Qatar coastal waters were reported by Rivers et al. (2019a) for a period between April of 2016 and April 2017. Water salinity for coastal regions of Qatar, including the Khor Al Adaid, were also reported for that time period by Rivers et al. (2019a). Measured air temperature in southern Qatar fluctuated fluctuates between 17 °C in winter and 36 °C in summer, and relative humidity ranged ranges between 32% and 65% (Rivers et al., 2019a). Qatar is influenced by two wind systems. The dominant winds are the northwesterly "shamal" wind" which reaches peak strengths in the late spring and summer (Yu et al., 2016). These are supplemented by the southwest monsoons, which are also a summer wind (Houbolt, 1957; Purser and Loreau, 1973). Average wind speed in southern Qatar during 2016–2017 varied between 2 and 4 m/s, and was dominantly from the north-northwest. Storms (i.e., periods lasting 1–5 days with exceptionally strong winds) occur a few times each year, mainly in the winter in association with the arrival of extra-tropical cold fronts (Murty and El-Sabh, 1989).

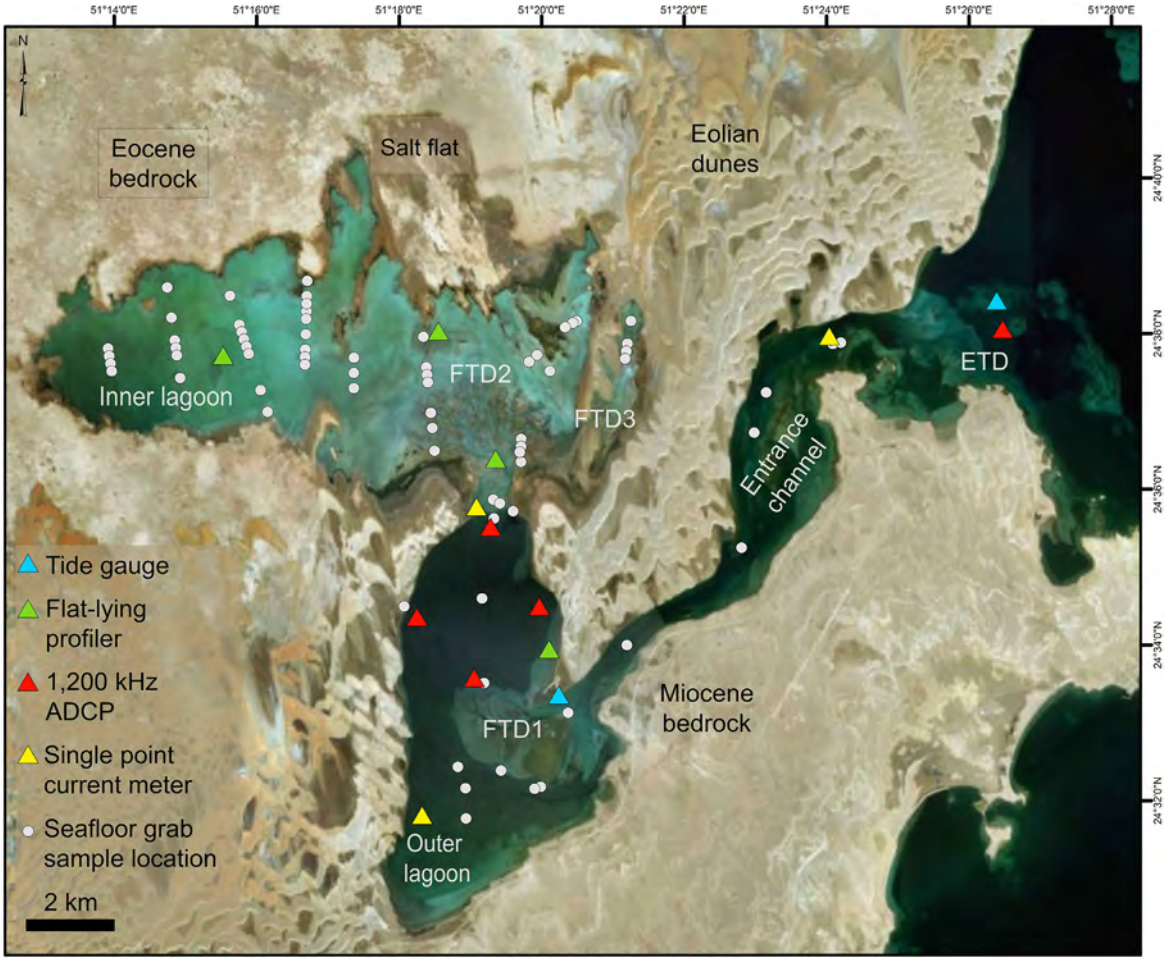

Fig. 3. Satellite image of the Khor Al Adaid showing the three morphological subdivisions, the Entrance Channel, Outer Lagoon, and Inner Lagoon, and the ages of the surrounding bedrock. Also shown are the locations of the various oceanographic measurements and of the sediment grab samples used to define the facies distribution (see Fig. 11).

Fig. 4. (A) Oblique airphoto showing eolian dunes migrating south-southeastward toward the Entrance Channel of the Khor Al Adaid. (B) Ground-level photo of eolian sand avalanching into the Entrance Channel. View to the SW.

During these storms, wind speeds can exceed 25 m/s (50 knots), with the winds coming mainly from the NW.

The surface seawater salinity of the open Arabian Gulf fronting the Khor Al Adaid channel and lagoon system during 2016–2017 ranged narrowly from 44 to 46 psu, whereas the water temperature varied between 18 °C and 30 °C (Rivers et al., 2019a). The inner part of the Khor Al Adaid is affected by extreme evaporation as a result of the arid climate and persistent wind regime. In the most isolated parts of the Inner Lagoon subtidal water salinity reaches 90 psu in the summer season and 70 psu in winter (Fig. 5; Rivers et al., 2019a). Rainfall is not observed to influence salinity values. Locally, restricted tidal ponds along the northern margin of the Inland Sea commonly reach gypsum or halite saturation (salinities of greater than 350 psu). The Outer Lagoon and Entrance Channel have measured surface salinities between 45 and 55 psu year around (Fig. 5). Measured water temperatures in the Inland Sea during the 2016–2017 sampling period varied between 20 and 31 °C.

Tides along the eastern coast of Qatar are mixed diurnal, with ranges of 1.1–2.3 m (Al-Yousef, 2003). Surface currents along this coast are tidally-driven and move generally southward and offshore at less than 10 cm/s (Pous et al., 2012; Pous et al., 2013; Lardner et al., 1988; Hunter, 1983; Vaselali and Vaselali, 2009; Elshorbagy et al., 2006). Because this coast is a lee coast relative to the dominant shamal wind, wave energy is low, with wave heights generally less than those of the open Arabian Gulf, which are reported to be less than 0.5 m (Loughland et al., 2012). The wave propagation direction is typically toward the south, causing longshore drift to be in this direction.

2.3. Previous sedimentological studies

The Khor Al Adaid (variably spelled Khor Al-Odaid and Khor Al-Udaid in older literature) was first described by various authors in Purser and Loreau (1973). These descriptions focussed primarily on the carbonate and evaporite components of the sediments. Clarke and Keij (1973) described the system as a highly-restricted environment, with shell-producing organisms being mostly limited to ostracods, and reported the presence of "thick gypsum crusts". They were likely referring only to the Inner Lagoon. Subtidal gypsum precipitation in the northern (leeward) margin of the Inner Lagoon was also reported by Loreau and Purser (1973). Purser and Loreau (1973) reported aragonitic

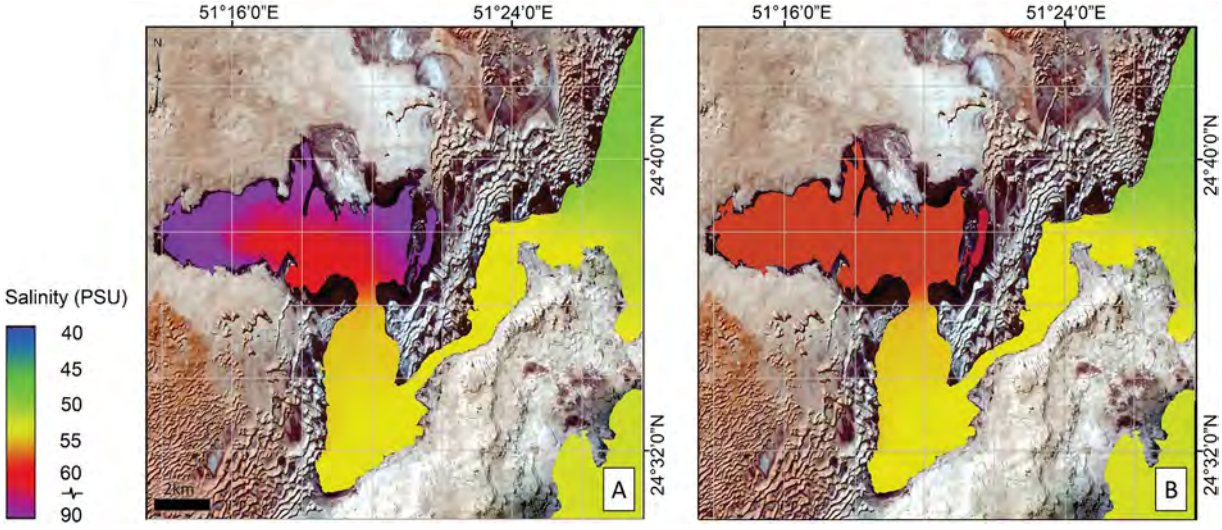

Fig. 5. Surface water salinity in A) summer, B) winter. These maps were created based on field sampling (2016 and 2017) around Khor Al Adaid and integration of contour trends from literature (Sadrinasab and Kenarkohi, 2009; Rezaei-Latifi, 2016; Rivers et al., 2019a).

crusts forming along coastal sand flats and on Cenozoic outcrops of the southern (less protected) margin of the Inner Lagoon. Ooids with tangential microstructure nucleating on quartz grains were reported to be forming in the moderately agitated waters on the western coast of the Outer Lagoon by Loreau and Purser (1973). They also observed scattered living corals and echinoids in the "southern" part of the system, here interpreted to refer to the Entrance Channel connecting the Outer Lagoon to the open Arabian Gulf. More recently Al-Khayat and Al-Mohannadi (2006) described molluscs living in the Entrance Channel. Paulo and Dittrich (2013) reported on dolomite forming in microbial mat communities of the Inner Lagoon.

By comparison, almost nothing has been published about the geomorphology and physical sedimentology of the system, or about the siliciclastic sands that dominate the deposits. The most well-known study is that of Shinn (1973) who described the influx of eolian sand into the northern side of the Entrance Channel and adjacent open-marine shoreline. He documented the progradation of the coast, in places by more than 1 km, by the deposition of eolian sand. The patterns of sand redistribution by tidal processes, and the spatial distribution of sediment composition throughout the system has not been examined in any of the previous studies.

3. Methodology

As a basis for all of the other studies carried out in the course of this research program, a bathymetric map was generated from high-resolution satellite imagery, ground-truthed using multibeam echosounder and single-point depth data. The satellite image used (WorldView-2, 2013) was obtained from DigitalGlobe Inc. (Westminster, CO, USA) and had a resolution of 2 × 2 m. The imagery was radiometrically calibrated, atmospherically corrected, mosaicked, and processed using an ENVI relative-water-depth algorithm to generate a map of water depths. This map was then trained using both multibeam echosounder measurements and individual sample point data to obtain the absolute depths (cf. Stumpf et al., 2003; Leon et al., 2006; Vahtmäe and Kutser, 2007; Legleiter et al., 2014; Eugenio et al., 2015; Pope et al., 2016; Warren et al., 2016). The procedure essentially converted colour tones into relative depths (lighter = shallower; darker = deeper). The water was generally clear because suspended sediment quantities were low, except in the very shallow Inner Lagoon. Consequently, the procedure gave good results in most areas. Unfortunately, factors other than water depth influence the colour as detected by the satellite (e.g., Maritorena et al., 1994; Stumpf et al., 2003). Seafloor sediment throughout the study area is all relatively light colored (quartz sand or carbonate mud; see below), so differences in reflectance are not a major complicating factor. The local presence of microbial mats was, however, a problem because they are dark colored and yield anomalously large depths by the method used here. Differences in the suspended-sediment concentration (SSC) in the water column also have a local influence on the results. Throughout the Entrance Channel and Outer Lagoon, SSCs are low and apparently uniform. In the very shallow Inner Lagoon by contrast, wave resuspension of the fine-grained carbonate mud gives the water a lighter colour. The images used in the depth determination were obtained early in the flooding tide, so clean, darker-colored water can be seen entering into and displacing the lighter-colored water at the entrance to the Inner Lagoon, especially at the tips of the distributary channels on the large flood-tidal delta (FTD 2; see below), creating anomalously deep areas. All of these depth anomalies are small and localized, and do not significantly detract significantly from the excellent results. Throughout most of the study area, depths are estimated to have an uncertainty of less than 25 cm.

Grab samples (n = 81) were collected from transect stations throughout the Entrance Channel and Inner and Outer Lagoons between 2015 and 2019, by wading in shallow water and from small boats in deeper water. Percentages of sedimentary components in each sample were estimated by inspecting the sand fraction through a binocular microscope using percentage charts. Optical characterization of these samples was augmented using petrographic thin sections. Inspection of the benthic habitats from which the samples were recovered was carried out using seafloor videos taken by an autonomous underwater vehicle (AUV). Mapping of sediment and habitat distribution was further refined though inspection of the satellite imagery used to create the bathymetric map.

During the fall of 2017 and the spring of 2018 physical and chemical oceanographic measurements were made using three Valeport single-point current meters, five Teledyne Acoustic Doppler Current Profilers (ADCP), two tide gauges, and six Aquadopp upward-looking current meters that were distributed throughout the Entrance Channel and Outer and Inner Lagoons (Fig. 3). Single-point current meters and the upwards-looking current meters also recorded temperature and salinity. Individual water-temperature and salinity measurements were obtained by wading and aboard a small boat using a Yellow Springs Instrument (YSI) EXO Water Quality Monitoring Platform. For samples with salinity greater than 70 psu as measured in the field, salinity was re-measured in the laboratory after dilution using a HACH HQ 440d multimeter.

A hydrodynamic model was generated to help in understanding water movement in the Khor Al Adaid system. The GEMSS (Generalized Environmental Modeling System for Surfacewaters; ERM, 2006) software was employed because it has been successfully used and calibrated in various locations around the Qatari coast (Kolluru et al., 2002; Adenekan et al., 2009; Febbo et al., 2012; Prakash and Kolluru, 2014; Yousif et al., 2018), and because it is capable of incorporating the influence of wind stress and salinity gradients. The measured and modelled bathymetry and shoreline configuration were used to constrain a non-orthogonal curvilinear grid, which consisted of 100 by 100 nodes, including inactive nodes on land that had a spacing of 204 m and a maximum of 18 layers with a vertical spacing of 1 m per layer. In shallow water, only the uppermost layers were activated. Measured, tidal-elevation data, wind speeds and directions, air temperature, relative humidity, and water temperature and salinity were utilized to build and calibrate the model. An upwind first-order computational scheme was used to solve the hydrodynamic differential equations, and the model was set up to incorporate hypersaline water densities (ERM, 2006). Because of the tight control by measured data, the model stabilizes after the first tide, and its output was used to generate maps and cross sections of current speeds and directions, water-surface elevations, and water density at various times over a representative tidal cycle.

Selected individual well-preserved and cement-free *Pirenella cingulata* gastropod shells and one coral fragment were cleaned with ethanol and deionized water and sent to Beta Analytic for ^{14}C dating. All ages are reported as calibrated ages in calendar years before present (yrs BP) referring to years before 1950 CE, or as "modern" if having formed after 1950 CE. For calibration the Marine13 calibration dataset was used (Reimer et al., 2013) and a local ΔR value of 180 ± 53 years (Southon et al., 2002) was applied.

4. Observations

4.1. General geomorphology and bathymetry

As noted above, the Khor Al Adaid consists of three parts, the Entrance Channel, the Outer Lagoon, and the Inner Lagoon which is farthest removed from the open Gulf. The NE-SW-trending Entrance Channel is 14.5 km long and is approximately parallel sided, varying between 0.55 km and 2.55 km in width (average 1.5 km). It is generally straight and runs parallel to the strike of the very gently, SE-dipping Miocene strata that underlie the area (Fig. 3). It does, however, deviate into a more north-south orientation part way along its length. The NW side is generally smooth in plain view, and has low relief, except where the lee faces of the south-southeasterly migrating eolian dunes

are coincident with the shoreline (Fig. 4). By contrast, the SE margin is rocky and irregular in plain view. The discontinuous thalwag of the Entrance Channel is mostly between 5 m and 7 m deep, and lies closer to the northern shore, particularly in the northern part of the channel, whereas extensive portions of the southern side of the Entrance Channel are less than 2 m deep. A diagonal chain of bars occupies the wider, north-south section of the channel. This feature is approximately 3.5 km in total length and 1.25 km in width. Toward the open Arabian Gulf, a small ebb-tidal delta occurs at the mouth of the channel, beyond which water depths fall quickly to greater than 15 m (Fig. 6). The location and shape of this channel may be influenced or controlled by high-angle normal faulting of the type documented elsewhere in the Qatar peninsula (Rivers and Larson, 2018).

The southwestern end of the Entrance Channel debouches into the north-south-elongate Outer Lagoon, which is approximately 10 km long and 4 km wide. A flood-tidal delta (termed FTD 1) approximately 12 km^2 in extent has formed in the Outer Lagoon at the end of the Entrance Channel, defining a distinct area where water depths are less than 2 m deep (Fig. 6). The southern part of the Outer Lagoon is likewise predominantly less than 2 m deep. The northern portion of the Outer Lagoon is significantly deeper, largely greater than 5 m, and reaching a maximum depth of 20.5 m. Except for the southern margin, the sides of this water body are steep, with very narrow nearshore areas. The origin of this depression is unknown, but it is too deep to be a simple continuation of any fluvial channel that once occupied the Entrance Channel. The shape and size of the Outer Lagoon are comparable to those of many of the larger sinkholes that occur on land (Howari et al., 2016; Engel et al., 2020), and this is our favored interpretation of its origin.

The Inner Lagoon is 14 km long in a NW-SE direction and less than 7 km wide, and is connected to the Outer Lagoon through a breached ridge of sand. A large, radial flood-tidal delta (approximately 14 km^2 in area, radius ca. 2 km) designated as FTD 2 has formed at its mouth (Figs. 3 and 6). This Lagoon has a very complex shape, being divided into three distinct sub-basins by elongate ridges of sand that trend NNE-SSW and are interpreted to be the remnants of linear draa (dune ridges). The connection between the western two sub-basins is relatively open, but the eastern-most sub-basin is connected to the main part of the Inner Lagoon only by a channel approximately 45 m wide. A small flood-tidal delta (FTD 3) has formed at the eastern end of this channel (Figs. 3 and 6). The Inner Lagoon is invariably less than 3 m in depth, with depths of greater than 2 m occurring only in the deepest part of the channels on the larger flood-tidal delta. The Inner Lagoon fronting the delta is less than 1.5 m deep at high tide, and is traversable by wading at low tide. This water body apparently formed by passive flooding of the low areas (troughs) between large, elongate draa. The carapace of these eolian dune ridges has been largely removed by deflation, except for remnant, small barchanoid dunes on the ridge

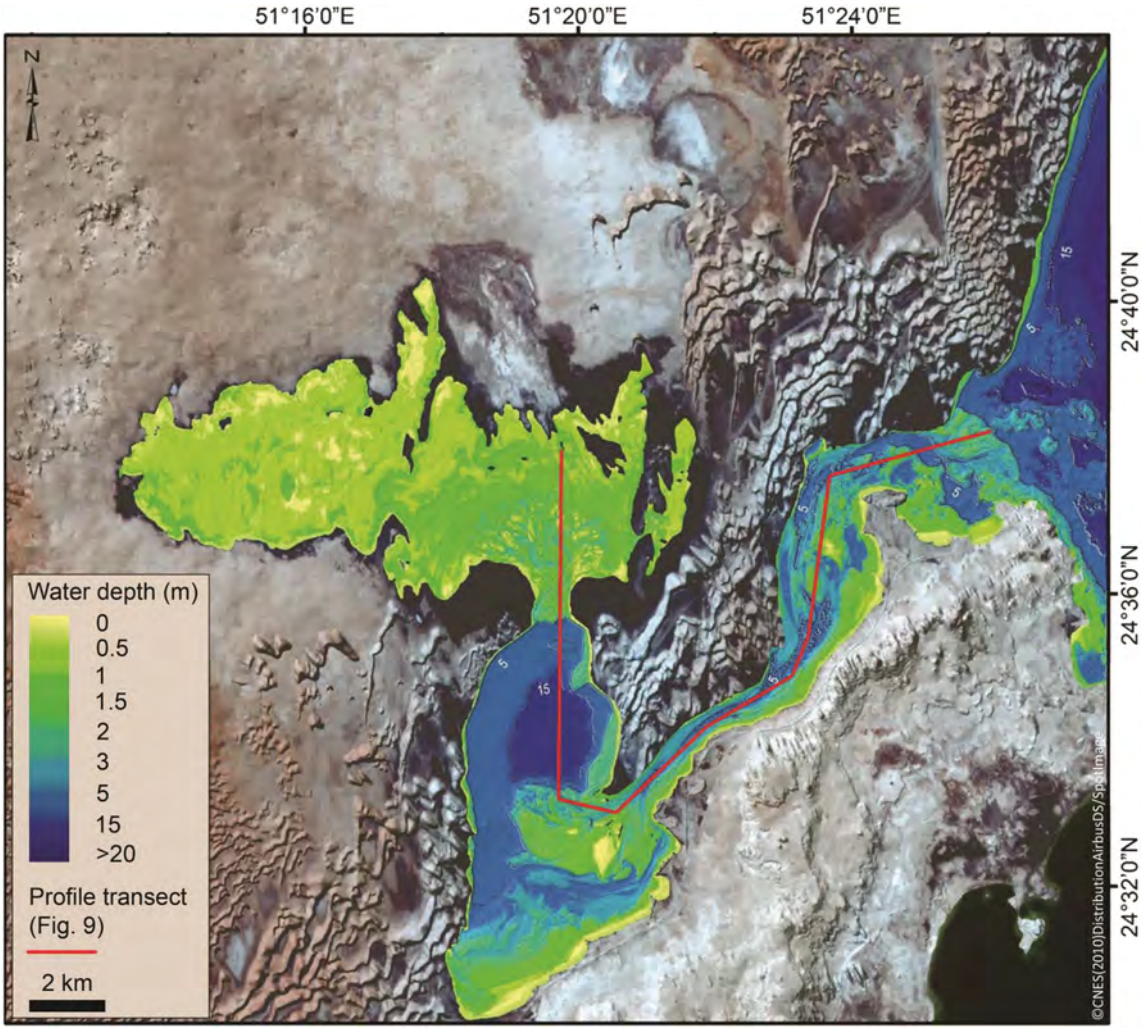

Fig. 6. Bathymetry of the Khor Al Adaid derived from satellite images, constrained by a large number of spot measurements. See text for description of the methodology used. The red line is the section used in Fig. 9 to illustrate the water-mass density structure in the Khor Al Adaid. (For interpretation of the references to colour in this figure legend, the reader is referred to the web version of this article.)

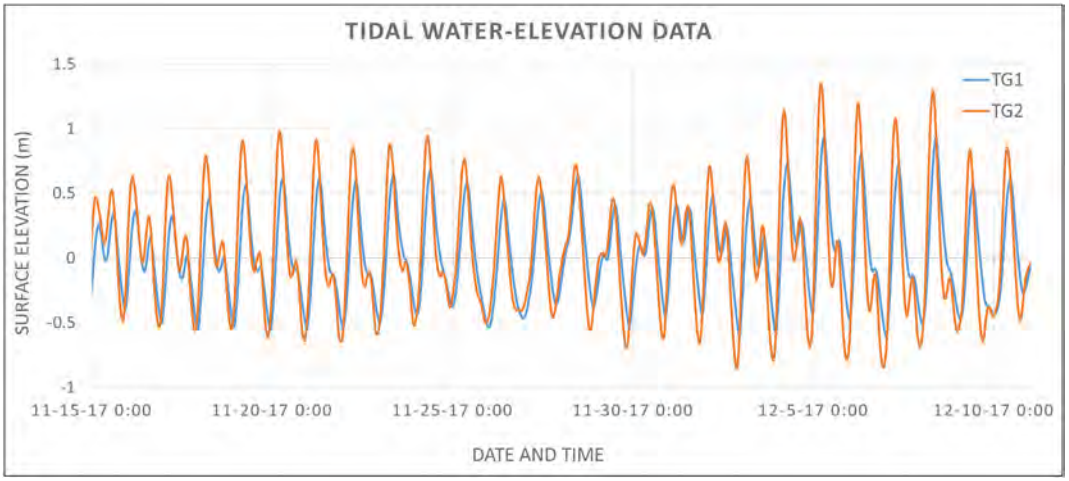

Fig. 7. Tidal water-elevation data for the period of November 15, 2017, until December 10, 2017. Tide gauge (TG) 1 was located at the southwestern end of the Entrance Channel, adjacent to the Outer Lagoon; TG2 was located at the mouth of the Entrance Channel, at the junction with the Arabian Gulf (see Fig. 3 for specific locations). The tides are dominated by the diurnal component, but with the semidiurnal component being most pronounced during and immediately after neap tides.

separating the small eastern sub-basin from the main lagoon, leaving only the subdued relief of the roots of these eolian bedforms as a control on the morphology of this lagoon.

4.2. Tides, density-driven circulation, and waves

The tidal system in the Khor Al Adaid is mixed, diurnally dominant (Fig. 7), and behaves as a progressive wave that decreases in amplitude as it propagates into the embayment. Thus, the tidal range decreases from 1 to 2 m over the neap-spring cycle at the mouth (Fig. 7), to 0.2–0.6 m in the Outer Lagoon, and to only 0.1–0.2 m in the Inner Lagoon. Tide-gauge and current-meter measurements, as well as the hydrodynamic model show that the crest of the tidal wave takes approximately 2–3 h to pass from the mouth of the system into the Outer Lagoon because of frictional retardation (Figs. 8, 9). This phase lag is also evident in the tidal-current data. When it is high tide at the mouth (Figs. 8A, 9A), the tidal currents are flowing landward throughout the Entrance Channel and both lagoons. During the early part of the falling tide at the mouth (Figs. 8B, 9B), flow is seaward but sluggish in the Entrance Channel, but the tide continues to rise in both lagoons, albeit slowly. By the time the trough of the tidal wave is at the mouth (i.e., at low tide there), the tide is ebbing throughout the system (Figs. 8C, 9C). During rising tide at the mouth, a complex system of currents is generated, with general landward flow established again in the Entrance Channel that is opposed by continued but weakening seaward flow through the lagoons (Figs. 8D, 9D).

The landward decrease in both the tidal range and tidal prism causes the tidal-current speeds to decrease into the embayment, a general trend that is strongly modified by changes in the local cross-sectional area. The fastest speeds occur in the narrow Entrance Channel and adjacent FTD1 where maximum speeds equal or exceed 1 m/s at the water surface (Table 1). There is then a sudden decrease in speeds into the broad Outer Lagoon to values of about 0.1 m/s. Current speeds increase again in the constriction at the entrance to the Inner Lagoon and over FTD2, reaching maximum surface speeds of ~0.3 m/s. Throughout the Inner Lagoon, maximum speeds are only rarely and locally greater than 0.15 m/s. As is the case with almost all shallow coastal embayments, the tidal wave is asymmetrical with a shorter rising limb and a longer falling limb, a pattern that develops because frictional retardation of the trough of the tidal wave is greater than the retardation of the crest (Dalrymple and Choi, 2003; Wang, 2012). Because of this asymmetry, current speeds are almost everywhere greater on the flooding tide than during the ebb, leading to a flood-tide dominance throughout most of the Khor Al Adaid, with maximum flood-tide speeds exceeding those of the ebb tide by 1.5–2.0 times, on average (Table 1).

The inward increase in salinity that characterizes the Khor Al Adaid in all seasons (Fig. 5) is a direct result of the landward decrease in tidal exchange that occurs in the context of the arid climate. Model calculations show that the residence time of water in the Entrance Channel averages 7 months, but increases to nearly one year in the Outer Lagoon, and to greater than 18 months in the Inner Lagoon (Table 1). As has been demonstrated by studies elsewhere, longer residence times (i.e., greater water "age") are directly associated with elevated salinities in estuaries (Largier et al., 1997; Kämpf and Ellis, 2015). The landward increase in salinity suggests that the system might exhibit reverse (or inverse) estuarine circulation, with inward flow at the surface and outward flow at the sea floor (Pritchard, 1955; cf. Postma, 1965; Largier et al., 1997; Ridd and Stieglitz, 2002; Winant and Gutiérrez de Velasco, 2003; Largier, 2010; Kämpf and Ellis, 2015) (Fig. 9A-D). Indeed, the Outer Lagoon exhibits a stratified water column, especially during and immediately after the ebb tide (Fig. 9C, D), with more saline bottom waters (55–60 psu) present below a depth of 5 m, and less saline surface waters (50–54 psu) above (Fig. 10). Results of the numerical modeling suggest that the denser bottom water originates in the Inner Lagoon and flows outward at the bottom during the ebb tide (Fig. 9A, C, D). This stratification is not as obvious and may not be present during the rising tide, however, because of turbulent mixing with incoming, less salty water by the tidal currents (Fig. 9B). In the Entrance Channel and Inner Lagoon, mixing by tidal currents and/or wave action in very shallow water yields a vertically homogeneous salinity distribution most of the time (Fig. 10). A weak vertical density gradient exists during the early phase of the rising tide in the landward part of the Entrance Channel (Fig. 9A), suggesting the presence of some inverse circulation at this time, although there is no clear reflection of this in either the measured or modelled tidal-current data. There is no indication of density stratification during the remainder of the tidal cycle (Fig. 9B–D).

When the northwesterly shamal winds blow at wind speeds of more than ca. 4 m/s, which is moderately common (Rivers et al., 2019a), wind shear generates surface flow that is generally in a southerly direction (i.e., down-wind and slightly to the right of the wind direction; cf. Jenkins, 1987). This flow, in turn, is believed to generate downwelling return flow at depth in the Outer Lagoon (see additional discussion in the section devoted to the morphology of the Outer Lagoon, 4.4.2). In addition to generating this wind-driven circulation, winds also generate waves, especially in the lagoons where the fetch is largest. Model outputs indicate that the wave heights reach approximately 0.5 m under exceptional circumstances; more commonly, they are only 0.1–0.2 m

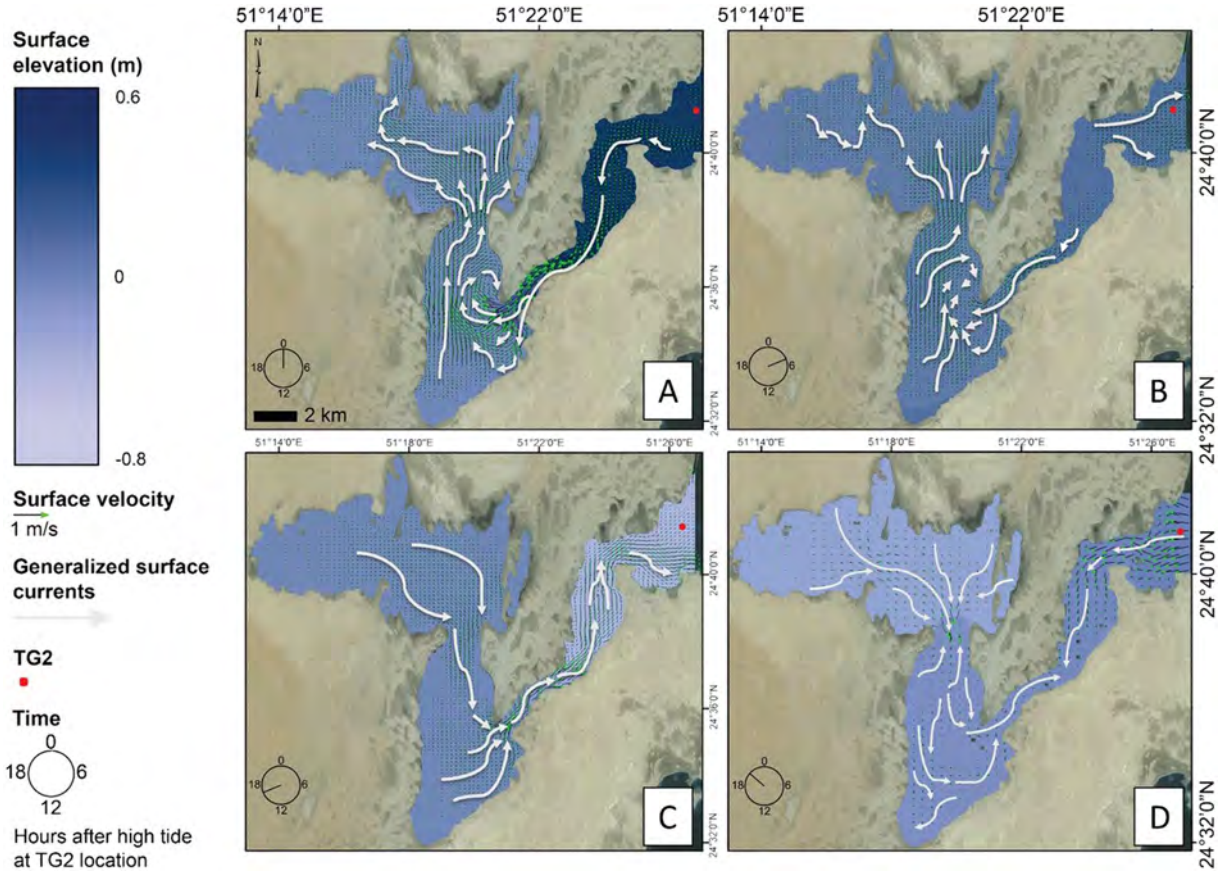

Fig. 8. Map of water-surface elevation (shades of blue) throughout the Khor Al Adaid and vectors showing surface currents (green arrows) at four times over a single tidal cycle, as generated by the hydrodynamic model; see text for additional description. Because the current vectors are too small to be visible easily throughout most of the system, generalized surface flow paths are shown by the gray arrows. (A) High tide at tide gauge (TG) 2 at the mouth of the Entrance Channel. Currents are directed landward throughout the entire system. (B) Approximately 4 h after panel A. The crest of the tidal wave is now located within the Entrance Channel. Flow is still landward in most of the system, but ebb flow has begun near the mouth. (C) Approximately 16 h after panel A. It is low tide at the mouth of the Entrance Channel, and the tide is ebbing throughout the entire system. (D) Twenty hours after panel A. The next flood tide as begun at the mouth of the system, but flow continues to ebb in the Outer and Inner Lagoons. See Fig. 9 for additional portrayal of the changes in water-surface profile over the tidal cycle. (For interpretation of the references to colour in this figure legend, the reader is referred to the web version of this article.)

high (Table 1). Because the dominant shamal winds blow from the N-NW, the most intense wave action in the lagoons is along their eastern and southern shorelines. At the mouth of the Entrance Channel, wave action is likely to be greater than elsewhere in the system because of exposure to waves in the open Gulf (Table 1). However, wave size is limited by the location in the lee of the Qatar peninsula. Morphological evidence of wave action there is restricted to the generation of a spit-like extension on the eastern flank of the ebb-tidal delta (Fig. 6).

4.3. Sedimentary components

4.3.1. Siliciclastic material

The overwhelmingly dominant constituent of the sediment throughout the Entrance Channel, around the margins of the Outer Lagoon, and in the three flood-tidal deltas is quartz-rich sand that is supplied by the eolian dunes. This sand consists mostly of rounded grains of quartz (~50%) with lesser quantities of feldspar (~30%) (Embabi and Ashour, 1993; Garzanti et al., 2013). These sands also include a smaller quantity of detrital calcite and dolomite grains that are likely derived from the carbonate bedrock (Eocene Dammam Formation) that underlies the eolian dunes. In general, the sands are poorly-sorted, with most samples ranging in size between upper fine-upper and lower coarse. The sands commonly have a small coarse tail composed of shell material. Modal sizes are in the lower-medium size range.

In addition to the quartz-rich sand, the wind also supplies small amounts of eolian dust that accumulates in the low-energy areas within the two lagoons. Characterization of the dust has been undertaken recently in Doha (Javed et al., 2017). The results show that modal sizes are in the range of 15–25 μm (i.e., medium silt). Calcite, dolomite, and quartz are the dominant minerals, with gypsum and halite being minor components. Accumulation rates in Doha, 70 km to the north of the study area, are between 100 and 150 mg/m^2/day.

4.3.2. Carbonate components

Uncompacted aragonitic mud is the dominant surficial sediment in the low-energy parts of both the Inner and Outer lagoons. This carbonate mud can occur in association with quartz-rich sand (forming a muddy sand) or as a distinct drape overlying sand. Distinct muddy layers include variable but subordinate amounts of very fine quartz sand and clay, both assumed to have been deposited by wind. The source of the carbonate component is unclear, but it is presumed to have formed in-situ rather than having been transported landward from the open Gulf, since waters of the Entrance Channel are always observed to be clear, and no mud accumulates in sheltered Entrance-Channel locations. Soft fecal pellets are common, being produced by the abundant gastropods that are observed grazing in the associated intertidal and shallow subtidal environments. Waters of the Inner lagoon are observed to be particularly turbid on windy days, and suspension of mud by wind-generated wave energy is assumed. Additional turbidity due to the formation of whitings (Shinn et al., 1989) related to spontaneous aragonite precipitation in the water column cannot be discounted.

A variety of sand- and gravel-sized carbonate grains form an important but minor constituent of most siliciclastic sands. Compared to

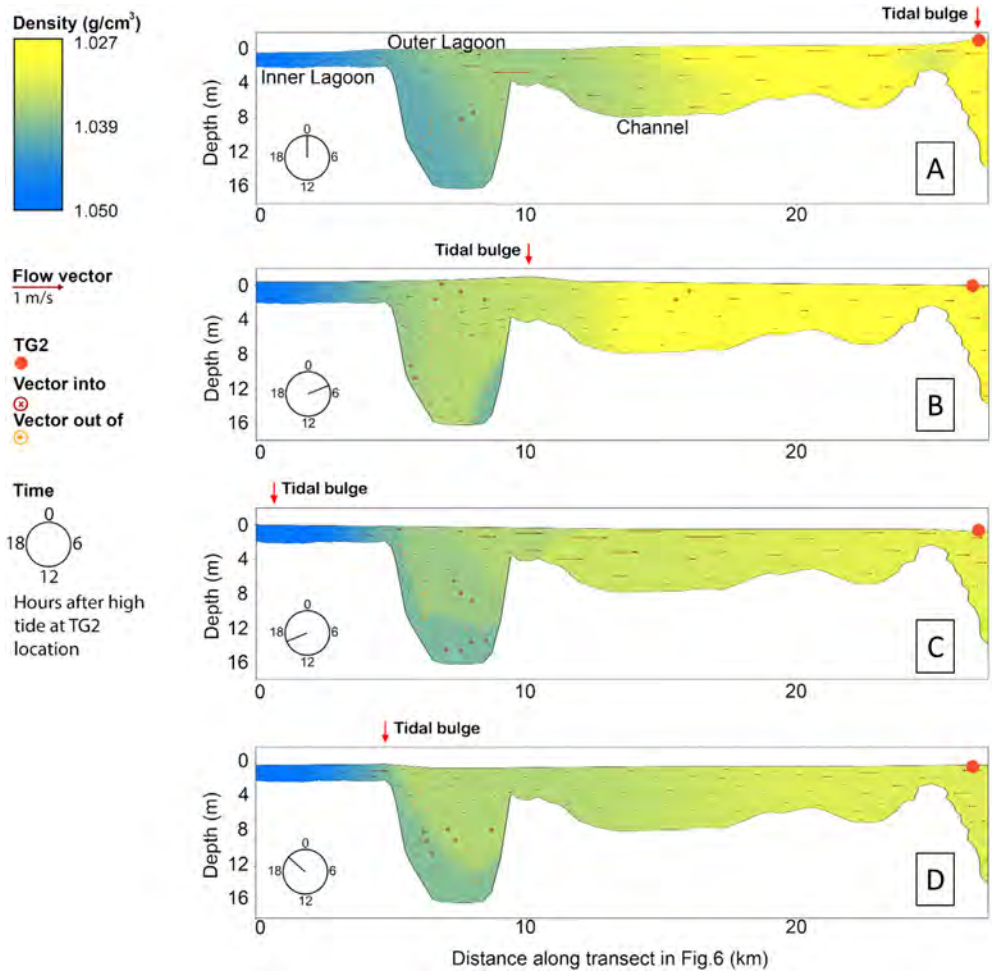

Fig. 9. Vertical profiles of bathymetry, water density structure, and current vectors along the longitudinal section shown by the red line in Fig. 6, at the same four times as portrayed in Fig. 8. The "tidal bulge" represents the location of the crest of the tidal wave. These plots were generated by the hydrodynamic model; see text for additional description. The water is effectively mixed by strong tidal currents in the Entrance Channel and density stratification is negligible. Wave action and tidal currents also lead to homogeneous vertical profiles in the very shallow Inner Lagoon. In the Outer Lagoon, however, denser water can be seen flowing seaward from the Inner Lagoon into the bottom of the Outer Lagoon at most stages of the tidal cycle, generating an inverse estuarine circulation in this area. See also Fig. 10. (For interpretation of the references to colour in this figure legend, the reader is referred to the web version of this article.)

open-marine areas, the diversity is low because of the elevated salinities and the frequent disturbance of the sandy sea floor by tidal currents. Common biogenic remains include dead corals and fragments thereof, coralline-algal fragments, whole and fragmented shells of infaunal and epifaunal bivalves, small gastropod shells, foraminifera tests, ostracod valves, and echinoid fragments. Benthic foraminifers are small, and occur in all sectors of the study area; common forms include rotalid, textularid, and miliolid. Coated grains and ooids are present in minor amounts in the sands from all parts of the system. Most ooids and coated grains have a tangential fabric, but radial types are also present in small numbers.

4.4. Depositional environments, geomorphology, and facies

Satellite-based investigation of the Khor Al Adaid, supplemented by seafloor photography, and sediment grab samples, has allowed for delineation of depositional environments and their facies in the Entrance Channel (3 facies), Outer Lagoon (5 facies), and Inner Lagoon (5 facies)

Table 1
Current speed and wave-height data as a function of location within the Khor Al Adaid embayment, as derived from direct measurements and the hydrodynamic model. ETD = ebb-tidal delta; FTD = flood-tidal delta.

System Component	Average (and maximum) flood tide current speed at the surface (m/s)	Average (and maximum) ebb tide current speed at the surface (m/s)	Average (and maximum) current speed at the seafloor (m/s)	Residence time (months)	Average (and maximum) wave height (m)
ETD	0.60 (0.80)	0.25 (0.40)	0.18 (0.30)	NA	0.60 (1.50)
Entrance Channel	0.40 (1.20)	0.20 (0.70)	0.25 (0.50)	6.8	0.15 (0.50)
FTD 1	0.40 (1.10)	0.20 (0.60)	0.22 (0.50)	NA	0.10 (0.60)
Outer Lagoon	0.06 (0.10)	0.03 (0.08)	0.01 (0.02)	12.8	0.18 (0.50)
FTD 2	0.10 (0.30)	0.06 (0.16)	0.07 (0.30)	NA	0.13 (0.50)
Inner Lagoon	0.09 (0.20)	0.05 (0.08)	0.05 (0.05)	18.6	0.08 (0.10)
FTD 3	0.08 (0.15)	0.04 (0.07)	0.03 (0.07)	NA	0.05 (0.10)

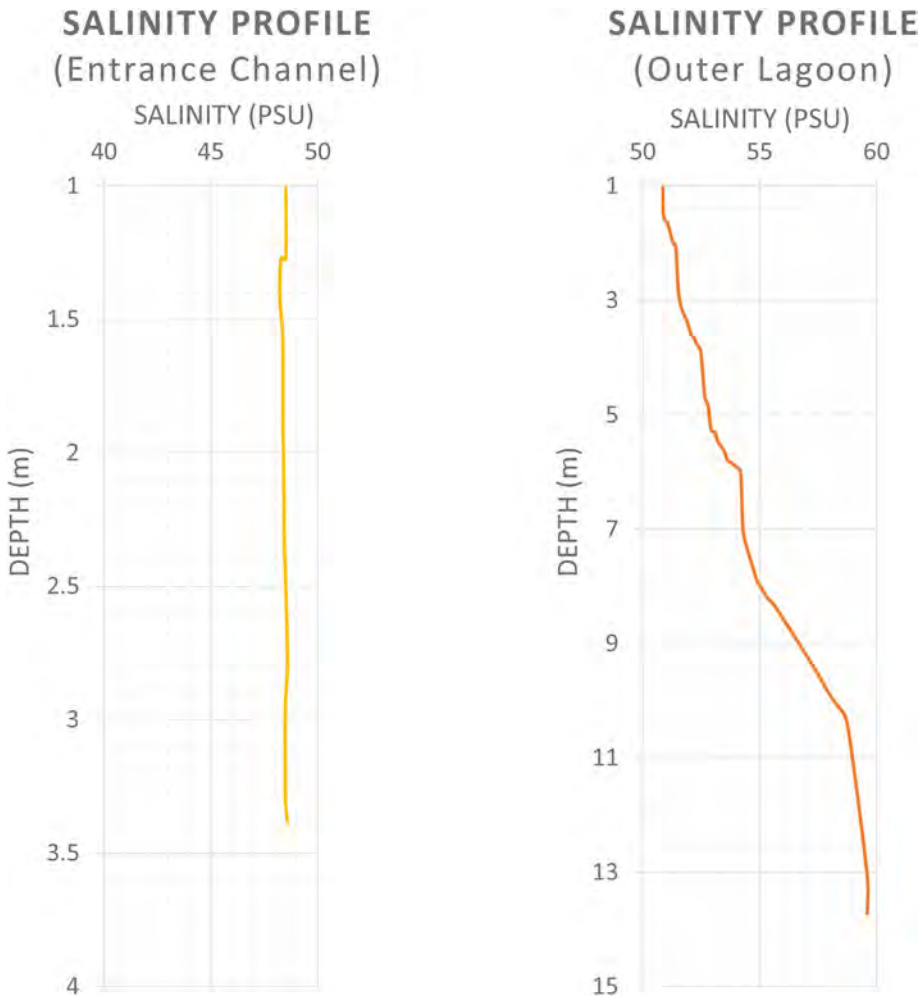

Fig. 10. Representative, measured vertical profiles of salinity in (A) the Entrance Channel and (B) the Outer Lagoon. There is no stratification evident in the Entrance Channel because of intense turbulent mixing, whereas pronounced salinity stratification occurs in the Outer Lagoon because of the inverse estuarine circulation illustrated in Fig. 9.

(Fig. 11; Table 2). Facies were delineated based on multiple parameters including association with morphological features (e.g., tidal deltas), water depth and current velocity, sedimentary components, the presence or absence of seagrass and macro-algae, and the nature of sedimentary structures. These facies and their associated attributes are summarized in Table 2.

4.4.1. Entrance Channel

Of the three sectors comprising the Khor Al Adaid, the Entrance Channel (Fig. 12) has the lowest average salinity, the highest tidal-current speeds, and the most dynamic sediment movement. It is also the main location where siliciclastic sand is supplied to the system by the migration of eolian dunes into the northwestern side of the Channel (Fig. 4). Bathymetric data (Fig. 12A) show the presence of a chain of shallow bars that trends diagonally across the Channel at the location where it takes a slight north-south jog (Figs. 12, 13A). This chain of bars is dissected by a series of small channels that are termed "swatchways" (Robinson, 1960; Dalrymple and Rhodes, 1995). On morphological grounds, supplemented by the asymmetry of dunes, the main channels that flank the bar chain have opposing directions of net sediment movement: the channel to the west (i.e., on the Qatar side) is flood-dominant, whereas the eastern channel is ebb-dominant. Over the entire length of the Entrance Channel, however, the main thalweg is flood-dominant. Other than the branch to the east of the bar chain, only the outermost 2–3 km is ebb dominant where it supplies sediment to a small ebb-tidal delta. The main flood-dominant thalweg is flanked locally by short ebb-dominant channels that terminate in a J-shaped bar at their seaward end. By analogy with the headward-terminating "flood barbs" that characterize many tide-dominated estuaries (Robinson, 1960; Dalrymple and Rhodes, 1995; Dalrymple et al., 2012), these short channels are here called "ebb barbs" (Fig. 13B). The bars that occur at the termination of these channels have a short flow-transverse segment that is the topographically highest part of the bar; these segments commonly connect to the margins of the channel. The flow-parallel portion of these bars (the long stroke of the "J") separates the ebb- and flood-dominant channels, and gradually tapers out in the landward direction. Successive ebb barbs are generally disposed on alternate sides of the main thalweg, just as flood-barbs are in tide-dominant estuaries (Dalrymple et al., 2012).

Within this complex mosaic of channels and bars, three broad sedimentary environments and facies can be defined in the Entrance Channel (EC): 1) EC1-active channels and bars with mobile sandy substrates; 2) EC2-seagrass/algal banks that form on sediment lobes and bars between active channels; and 3) EC3-small, isolated coral-bearing reefs (Table 2; Fig. 12B). The sediment in the active channels (facies EC1) consists predominantly of eolian-supplied quartz-rich sands. Bivalve fragments and other skeletal debris make up only a minor component of the channel deposits (Table 2), but are most abundant in the bedform troughs (Fig. 14A), and in sediment-starved areas with sand ribbons (see below). Although not abundant, the faunal diversity is relatively high because of the low salinity (Fig. 5). Small numbers of non-skeletal grains, including aragonite-coated quartz grains, are also observed. Because of the strong tidal currents (Figs. 8, 9), these sands are moved frequently, preventing the establishment of seagrass and algae.

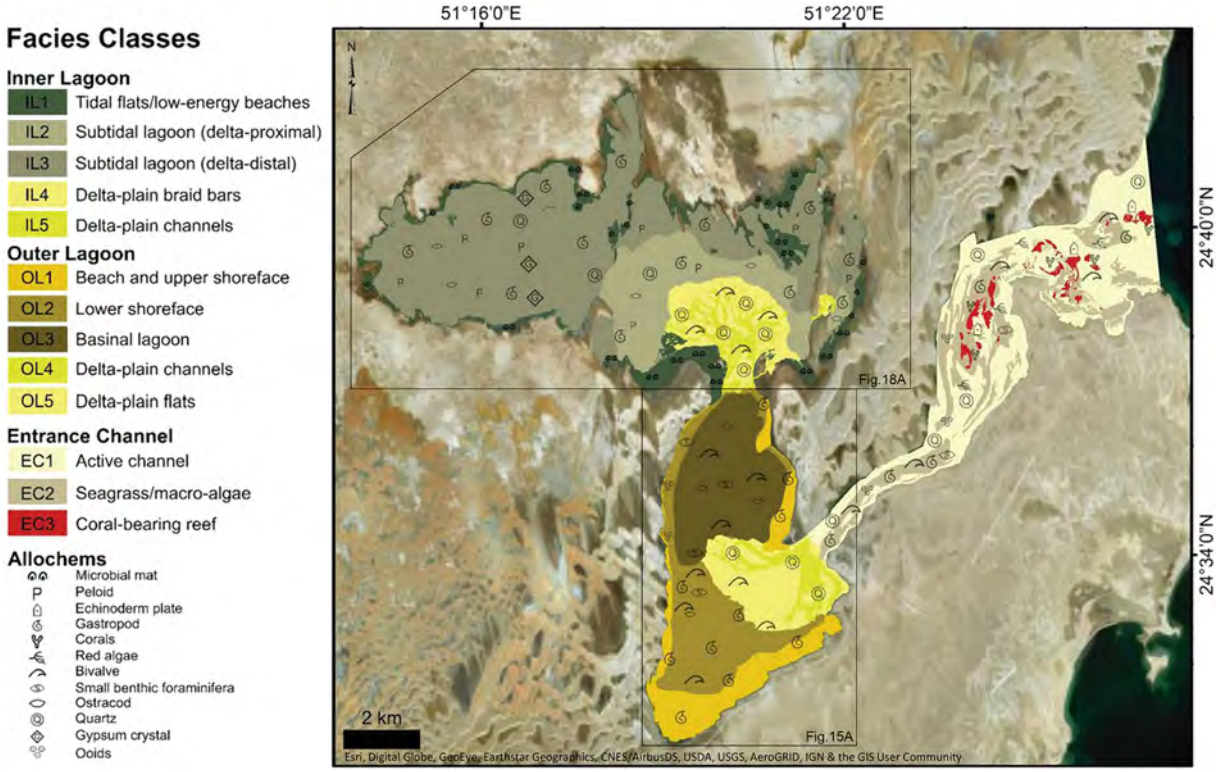

Fig. 11. Distribution of lithofacies throughout the Khor Al Adaid, based on the seafloor samples, the locations of which are shown in Fig. 3, and the analysis of satellite and seafloor images. See text for additional descriptions of the various sediment types. Boxes represent locations of bathymetric images in Figs. 15A and 18A.

A variety of current-generated bedforms are superimposed on the complex of sand bars and channels. Subaqueous dunes are widespread. In the deeper water of the main thalweg, dune wavelengths are of the order of 30–35 m, whereas smaller dunes occur in shallower areas flanking the main thalweg or in areas with a relative scarcity of sand. Dune heights are more difficult to determine accurately, but the largest dunes are typically 1.5–2.0 m high. Everywhere, their crests are oriented transverse to the channel axis and perpendicular to flow. The larger dunes are commonly covered with smaller dunes (i.e., they are compound dunes sensu Ashley (1990)). Centimeter-scale current ripples are widespread, both on the subaqueous dunes and along the shallower margins of the Entrance Channels, where current speeds are presumed to be too low to generate subaqueous dunes. Sand ribbons (Fig. 13A, B) oriented parallel to flow, and with lengths extending 100 s of meters, are also common bedforms within the active channels, in areas lacking sufficient sand to generate subaqueous dunes (Kenyon, 1970; McLean, 1981). Because the subaqueous dunes require a significant amount of sand to form, they are most abundantly developed along the Qatari side of the Channel along its entire length, and are relatively less common on the Saudi Arabian side. There, sand ribbons are widespread because of the limited availability of sand. Bedrock outcrops are also more common on the Saudi Arabian side of the Channel. At a smaller scale, the largest sand accumulations occur within the J-shaped bars that occur in the bedload-convergence zones between the through-going flood-dominant thalweg and the seaward-terminating ebb barbs (Fig. 13B). Consequently, subaqueous dunes are most abundant and largest there, and are less common in the intervening areas.

Although not included as a separate facies, the propagation of eolian dunes into the northwestern side of the Entrance Channel (Fig. 3) is likely to have developed a succession similar to the one documented by Shinn (1973) from the open-marine coast to the north of the Khor Al Adaid. The main difference that the succession in the Entrance Channel will show from that described by Shinn (1973) will be that the steeply dipping accretional bedding will downlap onto, or interfinger with, cross-bedded sand formed by migration of the subaqueous dunes along the axis of the Channel.

Meadows of seagrass, including *Halodule uninervis* (Fig. 14B) and *Halophila ovalis*, and both non-calcareous (*Chaetomorpha* and *Cladophora*) and calcareous green (*Acetabularia*) algae (facies EC2; Fig. 14C) are observed on the seafloor in less active portions of the Entrance Channel system, along sand lobes and bars between active channels. Surface sedimentary structures are not obvious due to the seagrass cover that are interpreted to have become established because of less frequent sediment movement. Sediments associated with these environments are shell-rich siliciclastic sands containing small amounts of aragonitic mud. Skeletal grains include bivalve shells and fragments thereof, particularly the clams *Dosinia erythra* associated with seagrass, and *Brachidontes variabilis* associated with non-calcareous algae. Other allochems include gastropods, coralline algal fragments, tests of small benthic foraminifera, ostracods, and echinoid fragments.

Coral-bearing patch reefs (facies EC3), typically 100 s of m^2 in extent and commonly elongated in the direction of the tidal currents (Fig. 12B), are only present in the northeastern portion of the channel system, close to the open Arabian Gulf. The corals belong to the *Porites* and *Acropora* genera, and are, with few exceptions, dead (Fig. 14D). ^{14}C-dating of bleached coral fragments demonstrates that they were living within the past 150 years. These fossil corals are encrusted with living red algae and soft sponges, and have been colonized by living *Pinctada* oysters (Fig. 14E). Non-calcareous green algae is also commonly observed, growing on fossil corals. Sediments flanking the reefs are grainy, being rich in skeletal debris, with minor amounts of fine to coarse quartz-rich sand. Fossils in these sands include fragments of encrusting red algae and corals, bivalves, gastropods, and encrusting worm tubes. Echinoids are commonly observed grazing near the reefs, and their remains are present in the sedimentary assemblage. Tests of small benthic foraminifera occur in small quantities.

Table 2
Description of the characteristics of the sedimentary environments and facies that occur within the Khor Al Adaid embayment. See text for additional descriptions and analysis.

Sector	Facies	Depth (m)	Sediment description	Skeletal components	Macrophytes and Non-calcareous algae	Sedimentary structures	Non-skeletal carbonate grains[a]	Gastropods (Family)	Bivalves (Species)	Small Benthic Foraminfera (Form)
Entrance Channel	EC1-active channel	0–7.0	Quartz sand with minor skeletal grains	Bivalves (commonly fragmented), gastropods, encrusting coralline algae fragments, echinoid spines, foraminferers	NA	2D dunes, sand ribbons, current ripples	Peloids, intraclasts, ooids/coated grains	Trochidae, Phasianellidae	*Brachidontes variabilis*, *Ervilia scaliola*, *Ervilia purpure*, *Pinctada radiata*, *Dosinia erythraea*, *Fulvia fragilis*	Rotaliida, Textulariida
	EC2-seagrass/macro-algae	2.0–6.0	Molluscan quartz sand with minor peloidal mud	Bivalves, gastropods, encrusting coralline algae fragments, foraminferers, ostracods, echinoids	Seagrass: *Halodule uninervis*, *Halophila ovalis*	NA-covered	Peloids, intraclasts	Potamididae, Scaphandridae, Trochidae, Haminoeidae, Phasianellidae	*Brachidontes variabilis*, *Ervilia purpurea*, *Dosinia erythraea*, *Pteria aegyptiaca*, *Ervilia scaliola*, *Pinctada radiata*, *Fragum sueziense*	Rotaliida, Textulariida
	EC3-Coral-bearing reef	5.0–7.0	Coralgal boundstone encrusted by oysters, and associated near-reefal sand	Encrusting coralline algae fragments, coral, bivalves, gastropods, formainiferers, serpulid worms tubes	NA	Reef	Intraclasts	Potamididae, Phasianellidae	*Pinctada radiata*, *Chama pacifica*, *Ervilia purpurea*, *Brachidontes variabilis*	Miliolida, Rotaliida
Outer Lagoon	OL1-beach and upper shoreface	0–2.0	Quartz sand with minor molluscs	Gastropods	NA	Ripples	Ooids (minor)	Potamididae	NA	NA
	OL2-lower shoreface	2.0–5.0	Carbonate mud with skeletal debris (wackestone)	Bivalves, encrusting coralline algae fragments, gastropods, foraminifers, ostracods	Seagrass: Halodule uninervis, Halophila ovalis	Bivalve burrows, gastropod grazing traces	Peloids	Potamididae, Phasianellidae, Columbellidae, Trochidae	*Brachidontes variabilis*, *Pelecyora ceylonica*, *Jitlada arsinoensis*	Millioid, Textulariida, Rotaliida
	OL3-basinal lagoonal	5.0–20.0	Carbonate mud (wackestone/mudstone)	Foraminferers, ostracods, bivalves, echinoids	NA	Bivalve burrows	Peloids	Potamididae	*Fulvia fragilis*, *Pelecyora ceylonica*, *Amiantus umbonella*	Millioid, Rotaliida, Textulariida
	OL4-delta-plain channels	0–2.0	Quartz sand with minor skeletal grains	Encrusting coralline algae fragments, gastropods	NA	2D dunes, 3D dunes, current ripples	Intraclasts, peloids, ooids	NA	NA	NA
	OL5-delta-plain flats	0–1.5	Molluscan quartz sand with minor peloidal mud	Encrusting coralline algae fragments, foraminferers, ostracods, bivalves, gastropods	NA	Ripples	Peloids	Columbellidae, Potamididae, Phasianellidae, Haminoeidae, Trochidae	*Fulvia fragilis*, *Amiantus umbonella*, *Jitlada arsinoensis*, *Pelecyora ceylonica*, *Brachidontes variabilis*	Rotaliida, Millioid, Textulariida
Inner lagoon	IL1-tidal flats/low-energy beachs	0–0.5	Unlithified microbial mats of variable thickness overlying quartz-rich eolian sand	NA	NA	Organo-sedimentary laminations on flats and wave ripples on beaches	NA	Potamididae	NA	NA
	IL2-subtidal lagoon (delta-proximal)	0.5–1.3	Quartz sand with minor molluscs and peloidal mud	Bivalves, gastropods, foraminerfers	Seagrass: Halodule uninervis	Wave ripples, gastropod grazing traces, vertical worm burrows	Peloids, intraclasts, ooids/coated grains	Potamididae, Scaphandridae	*Pelecyora ceylonica*, *Amiantus umbonella*, *Jitlada arsinoensis*	Rotaliida, Miliolida
	IL3-subtidal lagoon (delta-distal)	0.5–1.3	Peloidal carboante mud (wackestone)	Ostracods, encrusting coralline algae fragments, gastropods, foraminferers	Sparse algae	Wave ripples, gastropod grazing traces, vertical worm burrows	Peloids, intraclasts	Potamididae, Scaphandridae	NA	Rotaliida, Textulariida, Miliolida
	IL4-delta-plain braid bars	0–1.0	Quartz sand with minor molluscs	Bivalves, encrusting coralline algae fragments	NA	Complex current ripples, incipient microbial mats at channel margins	Peloids, ooids	NA	*Pelecyora ceylonica*, *Amiantus umbonella*, *Ervilia purpurea*	NA
	IL5-delta-plain channels	0.5–2.0	Quartz sand with minor molluscs	Bivalves (commonly fragmented), gastropods	NA	2D dunes, 3D dunes, current ripples	Peloids, intraclasts	Potamididae, Columbellidae	*Pelecyora ceylonica*, *Brachidontes variabilis*, *Amiantus umbonella*, *Jitlada arsinoensis*	NA

[a] Eocene and Miocene clasts commonly form 10% of quartz sand.

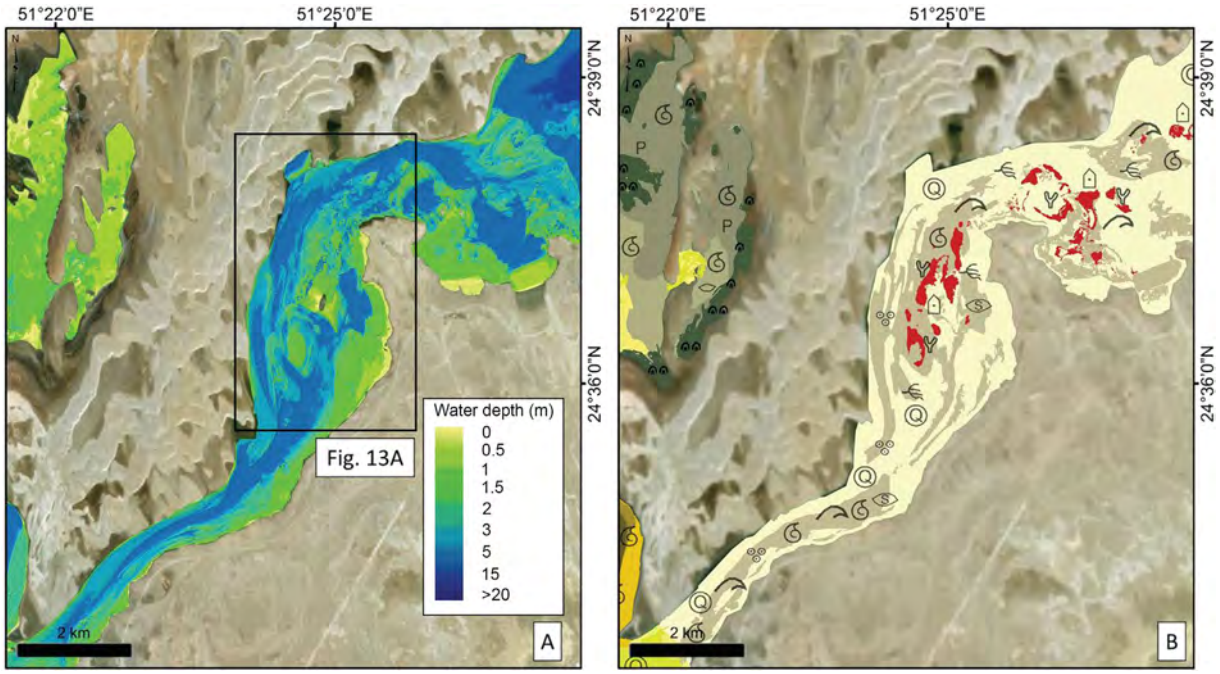

Fig. 12. (A) Bathymetry and (B) facies distribution (see Fig. 11 for legend) within the Entrance Channel of the Khor Al Adaid. In the area where the Channel turns into a more north-south orientation, a series of sand bars trends diagonally across the Channel. Details of this area are shown in Fig. 13A, the location of which is shown by the rectangle. A small ebb-tidal delta is present at the mouth of the Entrance Channel, in the upper right-hand corner of the image. Note that the reef facies is restricted to the more seaward parts of the Channel where salinity levels (see Fig. 5) are lowest. © COPYRIGHT 2018 DigitalGlobe, Inc.

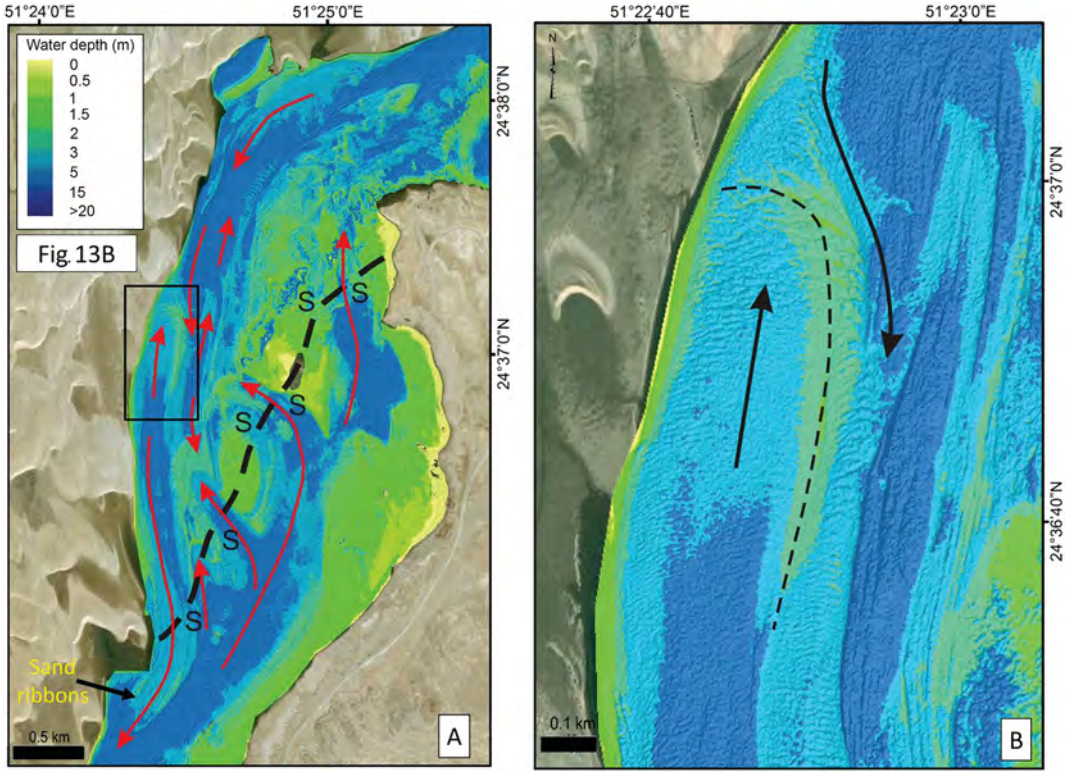

Fig. 13. (A) Bathymetry of the diagonal sand-bar complex (dashed black line) in the north-south segment of the Entrance Channel; see Fig. 12A for location. This "bar chain" (Dalrymple and Rhodes, 1995) is dissected by a series of channels that are termed "swatchways" (S). Red arrows show the directions of residual sediment movement, based on general bathymetric patterns and the facing direction of subaqueous dunes. Note the large-scale mutually evasive transport pattern relative to the bar chain, with net landward (flood-dominant) transport on its west side and net seaward (ebb-dominant) transport on its east side. A prominent field of flow-parallel sand ribbons is present on the flood-dominant sediment lobe at the bottom left-hand corner of the image. (B) Detailed bathymetry of one of the "ebb barbs" that are present along the sides of the flood-dominant thalweg of the Entrance Channel. (See panel A for location). Note the "J" shape of the bar, with a short east-west crest trending perpendicular to the channel margin and an elongate flow-parallel bar separating mutually evasive ebb-dominant (northward-directed) and flood-dominant (southward-directed) transport paths (black lines). Flow-transverse subaqueous dunes are visible on the bar crest, whereas flow-parallel sand ribbons are present in the main thalweg on the right side of the image. © COPYRIGHT 2018 DigitalGlobe, Inc. (For interpretation of the references to colour in this figure legend, the reader is referred to the web version of this article.)

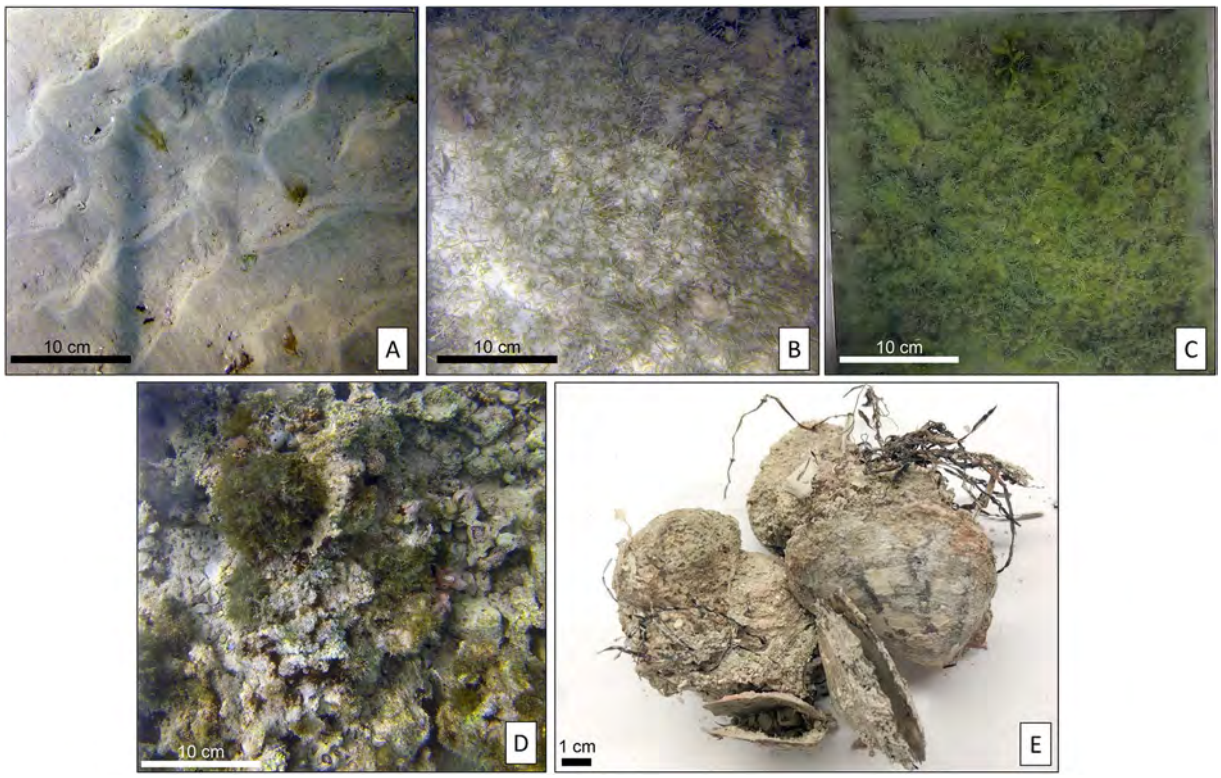

Fig. 14. Examples of sediment facies in the Entrance Channel. (A) Mobile quartz-rich sand with current ripples from within the active channel facies. Bivalve fragments are commonly observed in the ripple troughs. B) Meadows of *Halodule uninervis* between active channels. C) Turf of non-calcareous green algae *Chaetomorpha* and *Cladophora* in a less active area of the Entrance Channel. D) Bleached *Porites* and *Acropora* corals, in the northern portion of the Entrance Channel with calcareous green algae growth. E) Example of *Pinctata* oysters found living on bleached coral reefs. (For interpretation of the references to colour in this figure legend, the reader is referred to the web version of this article.)

4.4.2. Outer Lagoon

The Outer lagoon is the deepest of the water bodies comprising the Khor Al Adaid, and has the longest fetch parallel to the direction of the dominant shamal winds (Figs. 3, 6). Therefore, the influence of wave action is relatively more pronounced here than it is in the Inner Lagoon. Tidal-current speeds are generally weak, except where the Entrance Channel enters the Lagoon (Fig. 8; Table 1). The sedimentary environments of the Outer Lagoon (OL) and their associated facies can be delineated into: 1) the beach/upper shoreface (OL1) and the lower shoreface (OL2), respectively; 2) the deep-water, basinal lagoon (OL3); and 3) the flood-tidal delta (FTD1) at the mouth of the Entrance Channel that is divisible into delta-plain channels (OL4) and delta-plain flats (OL5) (Figs. 6, 15A; Table 2).

Beach and shoreface deposits (facies OL1 and OL2) ring the Outer Lagoon, but vary in width between only a few 100 s of meters in northern areas where the basin margins are steep, to over a kilometer along the southern, gentler shore (Fig. 15). The beach and nearshore/upper-shoreface zone (OL1) are the most energetic parts of the shoreline in areas removed from FTD 1. Typical beach lamination that dips gently offshore is present in the beach, and wave ripples are commonly present and generally oriented parallel to the shoreline in the shallow subtidal area. In the nearshore zone and upper shoreface to depths of ~2 m (facies OL1), various types of nearshore bars are present. Along the central southern coast, straight, shore-parallel ridges are present over a distance of ca. 4 km, and lie a few 10s of meters seaward of the shoreline (Fig. 15A–D) (cf., Dawson et al., 2002; Falqués et al., 2008; Ribas et al., 2017). Their relief is apparently only a few decimeters. The continuous nature of their crests reflects the fact that the waves approach the shoreline approximately orthogonally such that rip currents are not well developed (Davidson-Arnott, 2013). A second example of nearshore bars is present along the eastern shoreline of the Outer Lagoon. These features, which occur along two stretches of the shoreline with a total length of ca. 2 km, are linear to gently curved ridges that extend obliquely offshore from the beach (Fig. 15E). There are of the order of 100 ridges in these two fields. They occupy a zone approximately 80 m wide, and are spaced about 20 m apart. Ridges of this type are termed "transverse bars" or "finger bars" (Konicki and Holman, 2000; Garnier et al., 2006; Ribas et al., 2017, their Type 3 finger bars). They occur in areas of small, low-energy waves, especially in areas with a moderately strong longshore current that develops strong rip currents that occupy the ridge troughs In addition to these nearshore bars, parallel, 1-m-high sand ridges are observed in the wide upper shoreface of the southwestern corner of the Outer Lagoon (Fig. 15B). These ridges are oriented perpendicular to the southern shoreline and oblique to the western shore. They have a spacing of ~40–50 m, and are 300–800 m long, and satellite images suggest that they are at least locally mantled by subaqueous dunes. The origin of these ridges is unclear. One possibility is that they are the result of downwelling flow generated by the shamal wind, which causes a set-up at the southern corner of the Outer Lagoon, especially during periods when the wind is strongest. Qualitatively similar, shore-perpendicular features generated by downwelling flows have been documented in a variety of shoreface settings (e.g., Karl, 1980; Cacchione et al., 1984; Ferrini and Flood, 2005; Garnaud et al., 2005). Alternatively, they might represent a different form of transverse bars (Type 4 finger bars of Ribas et al., 2017), formed by shore-normal wave approach.

In the shallow waters of the beach, nearshore zone and upper shoreface (facies OL1), the sediment consists mainly of mud-free siliciclastic sand that has been supplied by the migration of eolian dunes into the Outer Lagoon. Bivalve shells (Fig. 16A–C, F) are the most abundant skeletal grains, together with *Pirenella cingulata* (previously *Cerithidea cingulata*) gastropods and their traces (Fig. 16D). Ooids have been reported locally (Loreau and Purser, 1973). Seagrass and macro algae, which are abundant in the lower shoreface (2–5 m depth), are not observed in shallow water. Sediments of the lower shoreface (facies OL2) generally consist of quartz-rich sand that

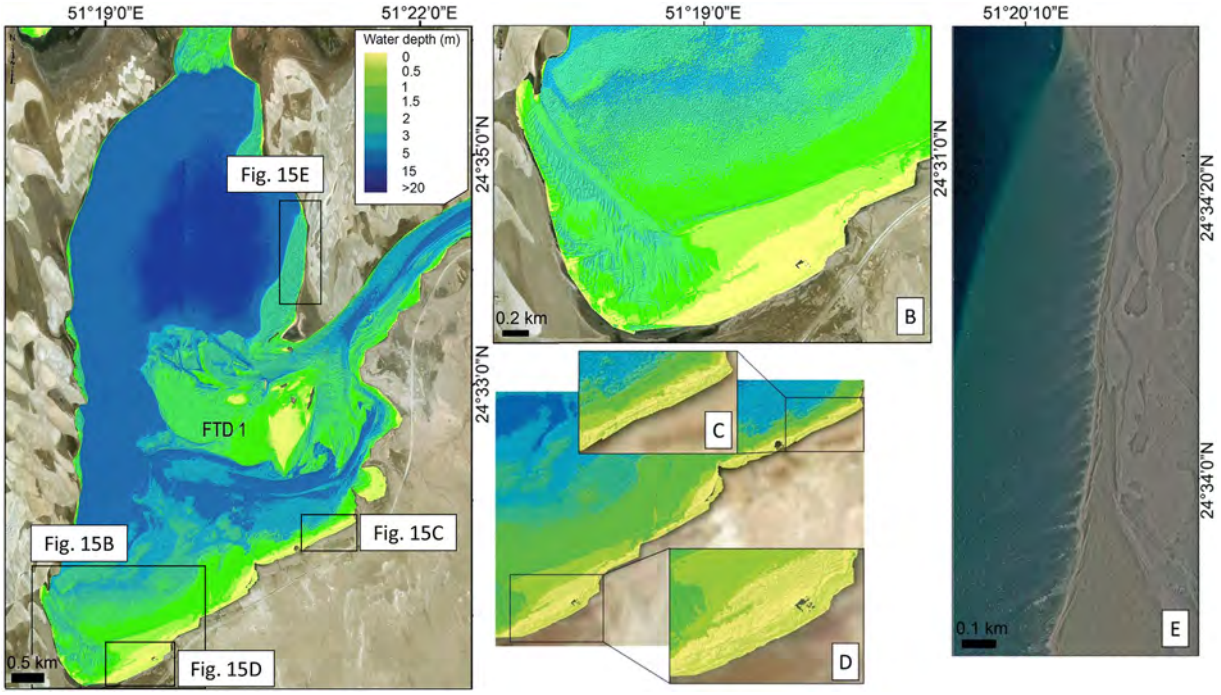

Fig. 15. Morphological features of the Outer Lagoon. (A) Bathymetry of the Outer Lagoon, showing the location of the flood-tidal delta (FTD 1) at the terminus the Entrance Channel, and the locations of the B-E parts of this figure (circled letters). Note that the deepest water occurs in the northern part of this lagoon, and that the eastern and western shorefaces are narrow, whereas the southern shoreface is broad and shallow. (B) Detailed bathymetry of the southwestern corner of the Outer Lagoon showing the shore-normal elongate ridges that are interpreted to be the result of wind-generated downwelling flow. (C) and (D) Portions of the southern margin of the Outer Lagoon illustrating the continuous, shore-parallel nearshore bars that characterize this shoreline. (E) Shore-oblique nearshore bars along the eastern margin of the Outer Lagoon.

contains variable amounts of aragonitic mud, the mixtures ranging in texture from muddy sand (shallower) to sandy mud (deeper). Shells commonly include molluscs, most conspicuously disarticulated, whole and fragmented *Pelecyora ceylonica* (Fig. 16A), *Brachidontes variabilis* (Fig. 16B), and *Jitlada arsinoensis* (Fig. 16C), as well as living *Pirenella cingulata* gastropods (Fig. 16D). Tests of small benthic foraminifera (rotalid and miliolid forms) and ostracods are present. Primary sedimentary structures are absent, but gastropod traces are common.

The basinal lagoon facies (OL3) occurs at depths of greater than 5 m, reaching a maximum depth of 20.5 m at the lagoon center (Fig. 15A). The depositional setting occurs below wave base, in waters that typically have elevated salinity (50–60 psu). The dominant sediment consists of carbonate mud, with a small admixture of silt-sized quartz that is presumably of eolian derivation. Skeletal debris is only sparsely observed at the surface, and commonly consists of bivalve fragments. A turf of non-calcareous green algae can variably be observed at depths of generally less than 10 m. Bivalve burrow structures are apparent at the sediment surface to all depths (Fig. 16E), and sediment samples demonstrate that small (cm-scale) cockles (family Cardiidae) are common; thus, the bottom waters are oxygenated, presumably because oxygenated high-salinity bottom water that originates in the Inner Lagoon is introduced by inverse estuarine circulation on a regular basis (Fig. 9). The sediments include rare ostrocods and small benthic foraminifera.

A large flood-tidal delta (FTD 1) is located where the Entrance Channel debouches into the Outer Lagoon (Fig. 17). Unlike the other two flood-tidal deltas (FTDs 2 and 3), FTD 1 is irregularly-shaped, extending further westward than southward or northward. Channels on the delta plain (facies OL4) are typically 10s of meters wide, and are observed to bifurcate, shallow, and broaden in the lagoonward direction. They are floored by quartz-rich sand forming straight-crested (2D) dunes that typically display a lagoonward migration direction. Delta-plain flats are commonly 100 s of meters wide, the highest parts of which extend into the intertidal zone and are frequently covered with non-calcareous green algae. The sediments comprising the flats that occupy most of the delta plain (facies OL5) are composed predominantly of quartz-rich sand that was presumably derived from the Entrance Channel by means of the flood-tidal transport dominance (Fig. 17). These sands also contain small amounts of carbonate mud, especially in topographically high areas, as well as common robust *Fulvia fragilis* bivalve shells (Fig. 16F).

An area in the south-central part of FTD 1 is anomalous because of its high elevation within the framework of tidal ranges: according to the bathymetry, it lies at or just below the high-tide level. Whereas it is normal for tidal flats to accrete to this level if mud is present (cf. Healy et al., 2002; Dalrymple, 2010), this is not easily possible in the absence of fine-grained sediment, because current speeds decrease toward the high-tide level and there is a limit above which sand cannot be transported. Therefore, in the absence of mud, the upper-intertidal zone is generally not filled with sediment (A. Canestrelli, University of Florida, Gainsville, U.S.A., Pers. Comm., 2019). We propose, therefore, that this diamond-shaped high area is an erosional remnant (Fig. 17) of an older phase of delta growth. The Entrance Channel would have been flooded and active as a tidal conduit shortly before and during the sea-level highstand that occurred from ca. 7000–1400 yrs. BP, at which time sea level was 1.5 m above the present-day elevation (Fig. 2). Since then, in response to the sea-level fall, FTD 1 appears to have been incised by the distributary channels, leaving the surface that formerly lay in the middle to lower intertidal zone stranded in the upper intertidal zone. At present, wave action appears to dominate sedimentation on these high areas, and those topographically lower areas that are protected from strong tidal currents, as indicated by the presence of straight-crested, wave-generated nearshore bars (cf. Davidson-Arnott, 2013; Ribas et al., 2017) on the western flank of the topographically high area (Fig. 17).

4.4.3. Inner Lagoon

The Inner Lagoon has the most complex outline of the sectors comprising the Khor Al Adaid, and is also the shallowest with a depth that is generally <1.5 m (Figs. 6, 18 A-D). Both of these characteristics are a result of flooding of the low-lying areas between a series of linear draa. The tidal range is significantly reduced relative to the mouth of the

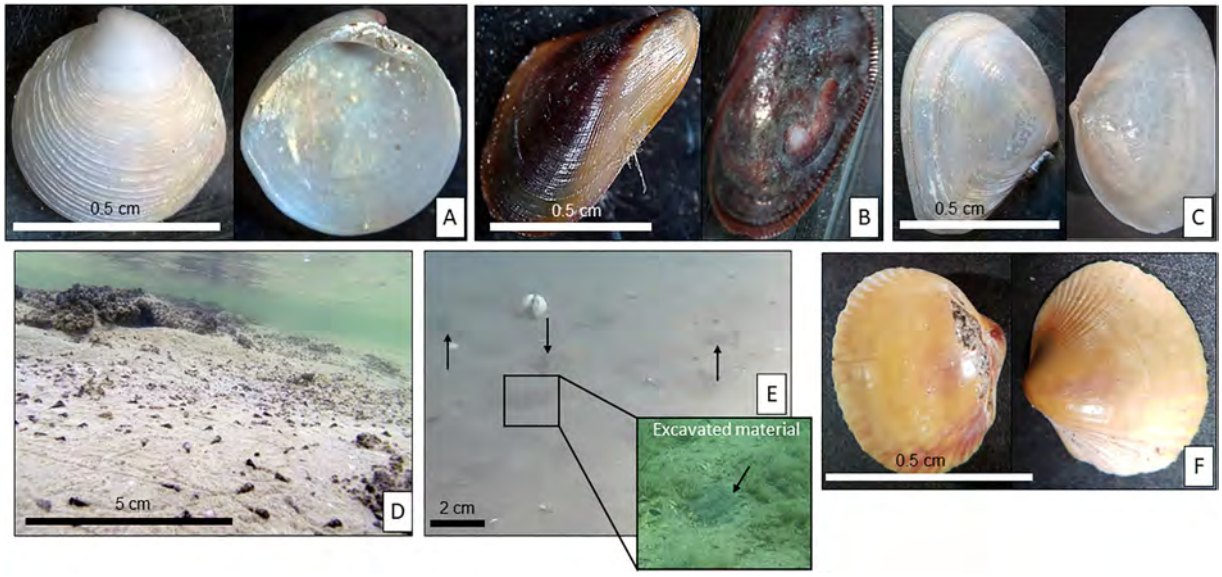

Fig. 16. Molluscs present in the Outer Lagoon. Bivalves commonly observed in the lower shoreface (OL2) facies including A) *Pelecyora ceylonica*, B) *Brachidontes variabilis*, and C) *Jitlada arsinoensis*. D) *Pirenella cingulata* gastropods common to the OL2 facies. (E) Bivalve burrow structures in the basinal lagoon facies (OL3). (F) *Fulvia fragilis* bivalve shells common to the delta-plain facies.

system (Table 1), and tidal-current transport of sediment is limited to the narrowest flow constrictions and the associated flood-tidal deltas. Elsewhere in this lagoon, wind-generated waves cause resuspension of the fine-grained bottom sediment. Salinities are always elevated relative to the remainder of the system (Fig. 5). Five broad sedimentary environments and facies are recognized in the Inner Lagoon (IL; Fig. 11; Table 2): 1) tidal flats and low-energy beaches (facies IL1) forming along the margins of the lagoon, which are commonly encrusted with microbial mats of varying morphology and thickness; 2) a sandy, shallow, subtidal lagoon floor found proximal to FTD 2 (facies IL2); 3) a muddy, extensive, shallow subtidal lagoon distal to FTD 2 (facies IL3); as well as 4) higher-energy braid bars on the delta plain (IL4) of the flood-tidal deltas (FTDs 2 and 3); and 5) distributary channels (IL5) on the delta plain of the flood-tidal deltas (FTDs 2 and 3; Fig. 18B, C), that are located at the landward side of flow constrictions.

Because the gradients of the lagoon margins are gentle around most of the shoreline, there is a broad, low-energy intertidal zone in most areas (facies IL1). Those that are more exposed to wave action have characteristics transitional to beaches. Microbial mats of varying morphologies are present on these tidal flats. In areas where the shoreline is composed of apparently barren sand (low-energy beaches, Fig. 18C), closer inspection typically reveals that the sands are stabilized by incipient microbial mats. In areas where mats are better developed, those marginal to the supratidal zone are only centimeters-thick, and typically have a blistered morphology (Fig. 19A). In the transition to the subtidal lagoon, the mats become decimeter-thick and, near the subtidal zone, they are polygonally-cracked (Fig. 19B). These leathery, organic structures are generally uncemented, and sediment-poor. Directly below the microbial mats, the substrate consists of loose quartz sand of eolian origin, with gypsum crystallites forming in situ. Two other much-less-common, yet lithified, microbial-mat morphologies have been identified in the Khor Al Adaid. Microbial mats with a "cat ear" morphology form in a few areas directly north of FTD2 (Fig. 19C), and "sand stromatolites" (Fig. 19D) form in association with a spring-fed tidal pond near the entrance to this lagoon. Waters at the base of this pond have been measured above 45 °C, and so the pond is inferred to be associated with a warm-water spring. The sand stromatolites are composed of lithified quartz sand, with cm-scale vertical columnar structures, cemented by micritic carbonate, presumed to be high-Mg calcite.

In local areas where the shoreline is exposed to more intense wave action (e.g., along the north-south western shore of the prominent elongate ridge that bisects the eastern part of the Inner Lagoon; Fig. 18C), complicated low-energy beaches are developed. Their large-scale geometry appears to be wave-formed and thus they seem to behave as beaches with various types of nearshore bars. The best-developed bars have a distinct cuspate shape, with a shore-normal amplitude of 20–25 m and an average spacing of ~150 m (Fig. 18C). They are called "sand waves" in the terminology of coastal morphology (Medellin et al., 2008; van den Berg et al., 2014), and are formed in areas with strongly oblique wave approach as is likely to be the case, given the orientation of the shoreline on which they occur relative to the Shamal wind (Fig. 18A, C). In other areas, such sand waves have been documented to migrate in the down-drift direction (i.e., to the south). Given the amount of microbial binding, however, only activity likely occurs only episodically, during periods with exceptionally strong winds and large waves. In the inter-storm periods microbial binding predominates. Determination of the extent to which this binding influences their morphology and mobility requires more study.

The floor of the subtidal lagoon includes two facies (IL2 and IL3) distinguished by their proximity to FTD 2. In areas distal to this flood-tidal delta (delta-distal facies IL3), a decimeter-thick layer of soft gray peloidal aragonitic mud covers much of the extensive low-energy subtidal lagoon floor, sparsely covered with a thin layer of non-calcareous, filamentous, green algae (Fig. 20A). The upper surface of this mud is presumably resuspended by strong wave action, leading to the turbid appearance of the water in satellite images. The mud is inferred to be at least partly composed of gastropod fecal pellets, generated by the innumerable *Pirenella cingulata* that can be observed grazing the seafloor, leaving meandering feeding traces. Commonly, millimeter-thick, discontinuous layers within the mud are partially cemented either by microcrystalline high-Mg calcite, or aragonite needles, resulting in a "corn-flake" texture underfoot when traversing the lagoon. Similar thin hardgrounds are typically observed at the base of the mud layer, overlying the substrate of quartz-rich sand assumed to be a relatively thin layer directly overlying bedrock (Fig. 20B) (Shinn, 1973). Vertical worm burrows are commonly observed within the near-surface sand and mud layers. In the central-western portion of the lagoon, small needles of gypsum have been observed in the sediment, presumably precipitated directly from the overlying seawater in the recent past. In the eastern region of the main lagoon, proximal to the delta (delta-proximal facies IL2), a distinct mud layer is generally absent, although the near-surface quartz sand

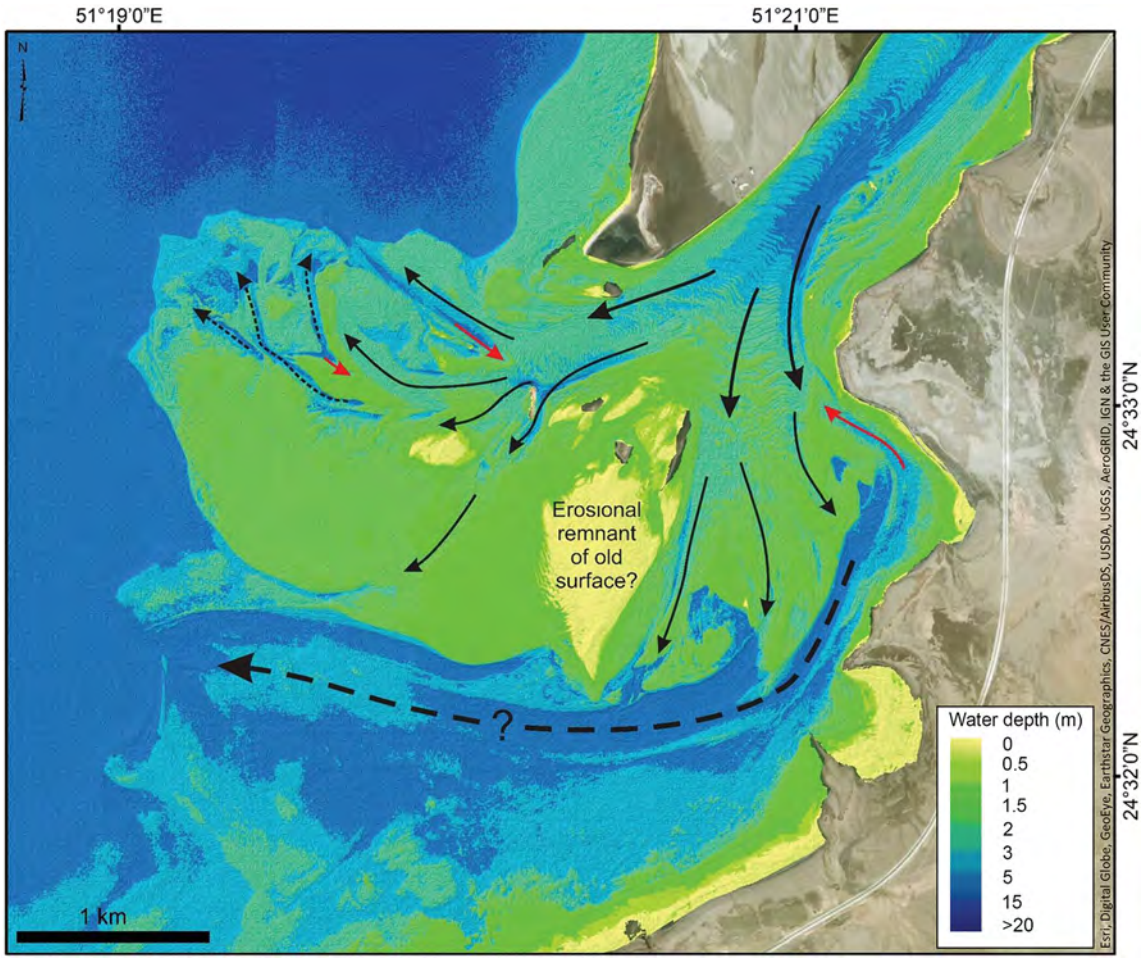

Fig. 17. Bathymetry of the flood-tidal delta at the junction between the Entrance Channel and the Outer Lagoon. Black arrows indicate areas that are inferred to have residual sediment-transport directions in the landward (flood) direction, whereas the red arrows indicate the small areas with an inferred ebb direction of residual transport. The imbalance in the abundance of the black and red arrows illustrates the flood-tide dominance of the system. The dashed black arrows indicate abandoned flood-tide distributary channels. The diamond-shaped shallow area in the central south part of the delta plain is composed of sand and sits so high in the upper intertidal zone that it is inferred to be a remnant of the delta surface that formed when sea level was 1.5–2 m higher (i.e., pre-1400 yrs. BP; Fig. 2). Linear, "nearshore bars" are present on the shallow part of the delta plain to the west of the remnant of the older surface. Note the very steep northern margin of the delta where it is prograding into deep water (see also Fig. 15A). (For interpretation of the references to colour in this figure legend, the reader is referred to the web version of this article.)

does include interstitial mud. In this same area sparse sea grass is commonly observed; such grass is absent from the areas with a muddy lagoon floor where IL3 occurs (Fig. 20C).

The larger of the two flood-tidal deltas (FTD 2) is located immediately landward of the entrance to the Inner Lagoon (Fig. 18B), whereas the smaller delta (FTD 3) lies to the east of the constriction connecting the main body of the Inner Lagoon with its smaller, eastern sub-basin (Fig. 18C). The top surface (i.e., the delta plain) of both deltas is criss-crossed by multiple channels (facies IL5), separated by lozenge-shaped bars (facies IL4) that give the delta plains a braided-channel pattern (Fig. 18B and C). Based on bar shapes, all of the surface of FTD 3, and most of FTD 2, is flood-dominant. The southern, proximal part of FTD 2 does, however, contain some small ebb-dominant lobate bars. On the whole, therefore, sediment transport on the deltas is effectively unidirectional because of the strong asymmetry of the tidal currents in this inland setting. Thus, it is reasonable to compare the shapes of these deltas with those of river-dominated fluvial deltas (cf. Bhattacharya, 2010). The margin of FTD 2 is smoothly arcuate with a regular semi-circular shape because it is building into an unconfined space (Fig. 18B). By contrast, the margin of FTD 3 is more linear because it is confined between the roots of the NNE-SSW-oriented draa that compartmentalize the Inner Lagoon (Fig. 18C). Both deltas lack the prominent bar fingers that are typical of birdfoot deltas and instead display a characteristic lobate form. Extensive research has shown that the difference in morphology between birdsfoot and lobate deltas is a direct result of the grain size of the sediment supplied to the channel mouths, with the birdsfoot shape occurring when the sediment contains a significant fraction of cohesive fine-grained (muddy) sediment, whereas the lobate shape occurs if the sediment is cohesionless (i.e., sandy) (Hoyal and Sheets, 2009; Edmonds and Slingerland, 2010; Caldwell and Edmonds, 2014; Burpee et al., 2015). Thus, the gross form of the flood-tidal deltas of the Inner Lagoon, which consist of sandy sediment, is consistent with the current understanding of the factors shaping river deltas. Although the delta margins are regular at the large scale, they are irregular at the finer scale, with the distributary-mouth protrusions extending ca. 100–150 m seaward of the inter-distributary embayments. Examination of the sequential images available in Google Earth shows that avulsions cause new distributaries to occupy former inter-distributary locations, ultimately leading to a net uniform progradation of the delta margin, and the stacking of individual lobes in a compensational style (cf. Straub et al., 2009; Bhattacharya, 2010; Wang et al., 2011).

The braid bars on the delta plain (facies IL4), which generally form bodies on the scale of 100–300 m in length, are commonly barren quartz sand, although thin microbial mats are observed in protected areas away from the influence of the stronger tidal currents that occur in the channels. Barren areas locally exhibit complex ripple patterns that are a result of the interaction of tidal currents and waves. Ooids occur in minor amounts, and there is a small admixture of sand-size

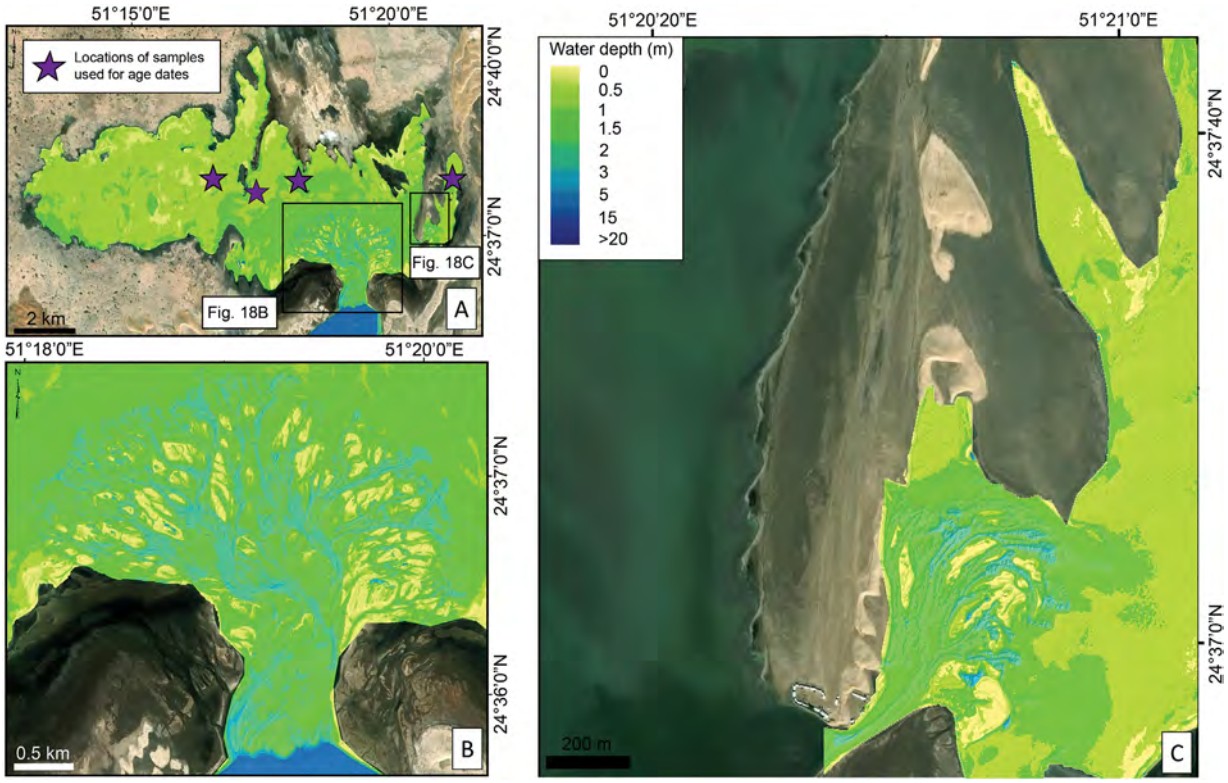

Fig. 18. (A) Bathymetry of the Inner Lagoon showing locations of flood tidal deltas. (B) Bathymetry of the flood-tidal delta at the entrance to the Inner Lagoon (FTD 2). (C) Bathymetry of FTD 3. Note the low-energy beaches with wave-formed bars on the western shore of the deflated dune stabilized by incipient microbial mats (black areas behind bars).

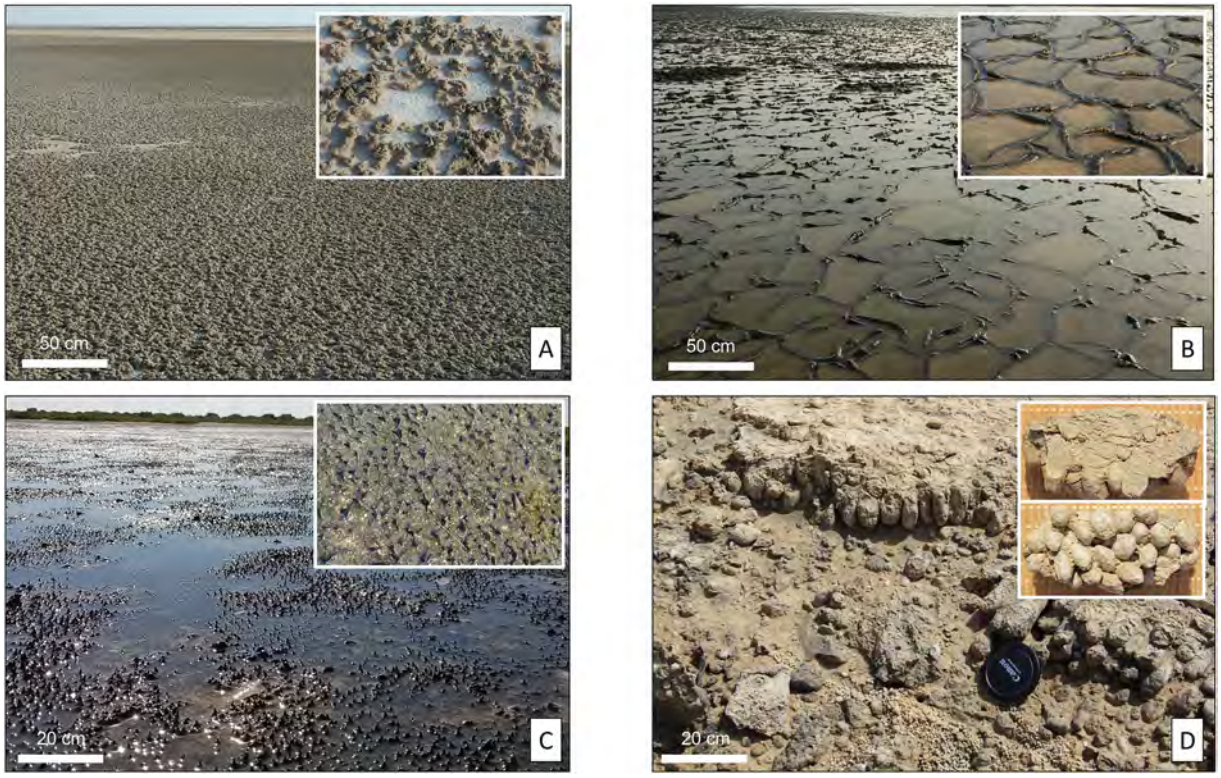

Fig. 19. Morphology of microbial mats of the Inner Lagoon. (A) Centimeters-thick blistered mats marginal to the supratidal zone. (B) Decimeter-thick polygonally-cracked mats of the lower intertidal zone. (C) Microbial mats with a "cat ear" morphology are found in intertidal areas north of FTD2. Example shown is from Al Ruwais area, in northern Qatar. (D) "Sand stromatolites" associated with a spring-fed tidal pond near the entrance to the Inner Lagoon. These columnar stromatolites are composed of lithified quartz sand.

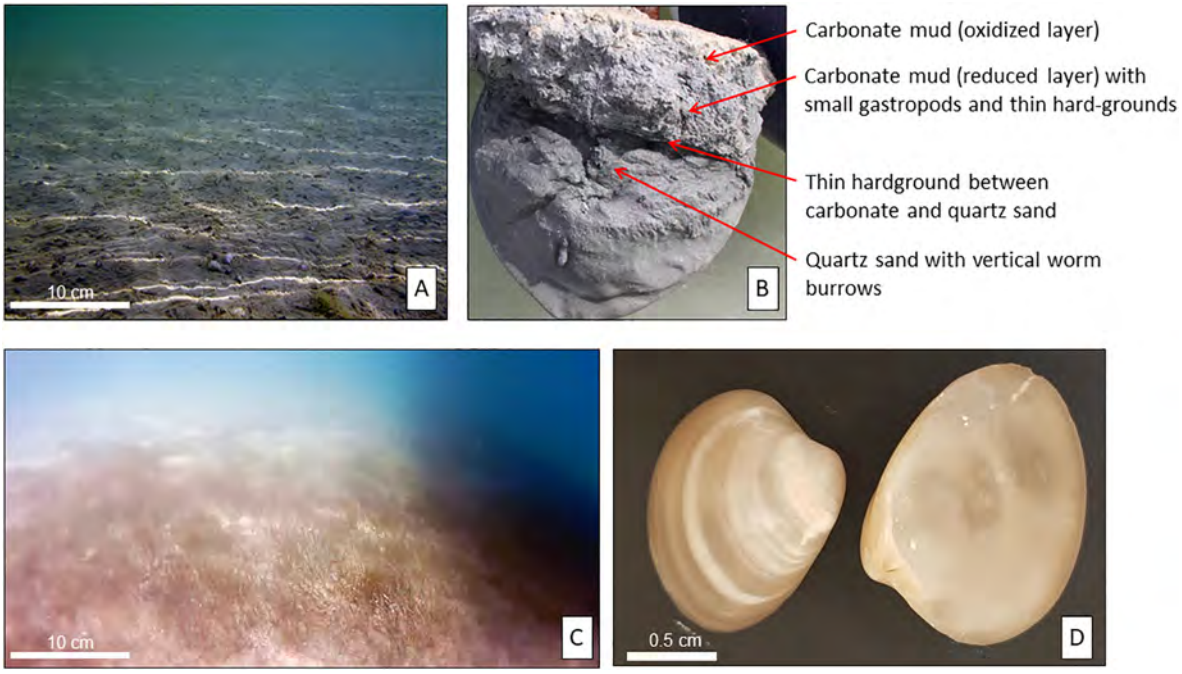

Fig. 20. (A) Bioturbated peloidal aragonitic mud of the delta distal facies (IL2) with a covering of spare non-calcareous green algae. (B) Image of muddy layer (as panel A) showing bioturbation and cementation (shovel shaft 5-cm wide). (C) Muddy quartz sands of the delta proximal facies (IL3) supporting seagrass growth. (D) *Amiantus umbonella*, a common bivalve of the Inner Lagoon delta plain. (For interpretation of the references to colour in this figure legend, the reader is referred to the web version of this article.)

fragments of bivalves and encrusting coralline algae (Table 2). The channels between the bars (facies IL5) become smaller as they bifurcate from the delta apex toward the delta margin, ranging from ca. 100 m wide and 2–3 m deep near the delta apex, to only 10–20 m wide and < 1 m deep near their terminus at the delta margin. Medium to large dunes (sensu Ashley, 1990) are observed in the proximal part of the channel network in FTD 2. In the more distal channels of FTD 2, and throughout the channels of FTD 3, dunes are not present; instead, the channel floors are covered by active current ripples that reverse with the changing tide. The sediments consist primarily of quartz-rich sand, and are largely devoid of skeletal grains. Shells of infaunal bivalves, particularly *Fulvia fragilis* and *Amiantus umbonella* (Fig. 20D) and fragments thereof, are present in sediments of the delta plain, as are minor amounts of other skeletal grains, intraclasts, peloids, and ooids.

Based on measurements made using historical aerial photography as well as more recent satellite imagery, FTD 2 has been growing larger

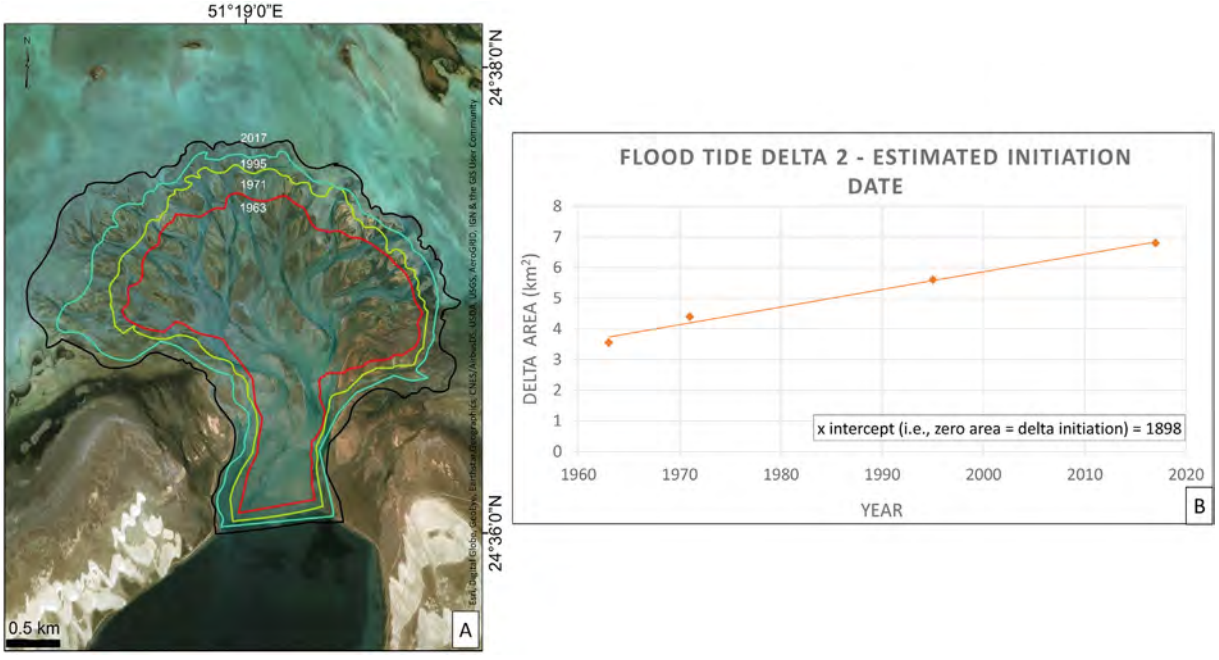

Fig. 21. (A) Satellite image of FTD 2 acquired in 2017, on which are superimposed the delta-margin outline in preceding years, showing the radial growth of the delta over the 54 years since 1963. (B) Plot of delta area as determined from the outlines in panel (A) as a function of calendar year. The red line is the best-fit regression line that has the equation given in the inset box. Extrapolation of this relationship to zero area (= inferred time of delta initiation) implies that the delta began to form in 1898. (For interpretation of the references to colour in this figure legend, the reader is referred to the web version of this article.)

and prograding into the Inner Lagoon since 1963 (the earliest available aerial photography) at an average rate ranging between 5 and 17 m/y depending on location around its periphery (Fig. 21A). A best-fit regression line for the plot of delta area vs time (Fig. 21B) indicates that the initiation of the delta (zero-area time intercept) occurred approximately in the year 1898. Carbon dating of four gastropod shells taken from within the muddy layer of the subtidal lagoon north and west of the delta (Fig. 18A) showed they are modern (having formed sometime after 1950 CE), supporting the possibility that the Inner Lagoon, as it is currently manifested, formed less than 200 years ago. The cause for the formation of the Inner Lagoon and the initiation of FTD2 is not known. Possible explanations include subsidence or autogenic breaching of the sand ridge, but there is no evidence to choose been these possibilities.

4.5. Environmental summary

The Khor Al Adaid is a morphologically complex marine embayment. This complexity occurs in part because of the shallow gradient of the bedrock surface (Eocene and Miocene carbonate rocks) over which the marine transgression has flooded, and because the various sectors of the system have different origins: the Entrance Channel is nearly linear because of fault control; the Outer Lagoon is ovoid, perhaps because it represents a flooded karst feature; and the Inner Lagoon is constrained to the low areas between a set of moribund eolian bedforms. Within the embayment, tidal currents are the dominant sediment-transporting agent, and yet the morphology does not conform to that of a tide-dominated estuarine system (Dalrymple et al., 1992, 2012). Instead, the existence of low-energy water bodies (lagoons) and flood-tidal deltas is more typical of wave-dominated estuaries, although the "barrier" at the mouth is not wave-built as it is in the classic model (Dalrymple et al., 1992), but is instead composed of the bedrock coasts to the north and south of the mouth of the Entrance Channel. Therefore, this system does not fall neatly into the existing process-morphological classification scheme for estuaries (Dalrymple et al., 1992) because of the bedrock constraint on its morphology.

Tidal-current energy and the associated high-energy (cross-bedded) sandy facies decrease in abundance inward because of the progressive decrease in the tidal range and tidal prism (Table 3). The nature of the channel deposits reflect this progressive decrease in tidal energy, from the widespread development of cross-bedded sands in the Entrance Channel and the delta-plain channels on FTD 1, to the restricted presence of cross-bedding in the proximal channels of FTD 2, to only rippled sands in the distal channels of FTD 2 and all of FTD 3.

Within the two lagoons, low-energy conditions prevail away from the shoreline and flood-tidal delta areas. Waves are important in both lagoons, generating beaches and wave-generated bedforms along the shorelines of the Outer Lagoon and locally in the Inner Lagoon, and causing resuspension of fine-grained sediment in the very shallow Inner Lagoon. Carbonate grains are present in most areas, typically as a minor constituent in high-energy settings (excepting the coral reefs in the outer part of the Entrance Channel), but dominating in areas of seagrass formation, or in the low-energy areas within both lagoons. The landward increase in salinity, as the isolation from open-marine waters increases, is reflected in the diversity of the benthic organisms present: corals once thrived in the seaward part of the Entrance Channel, whereas the fossils in the Inner Lagoon consist mainly of gastropods.

Table 3
Tidal range and tidal prism at the apex of each of the three flood-tidal deltas discussed in the text.

Delta	Tidal prism (m^3)	Tidal range (m)
FTD3	276,108	0.18
FTD2	6,410,447	0.35
FTD1	7,370,790	0.48

Microbial mats are extensively and exclusively developed in the Inner Lagoon, accompanied by the local presence of gypsum. The landward increase in salinity generates an inverse estuary, with evidence of weak seaward movement of bottom water from the Inner Lagoon into the deeper parts of the Outer Lagoon. This exchange prevents the bottom of the deep Outer Lagoon from becoming anoxic. Otherwise, there is no evidence of inverse estuarine circulation, presumably because the strong tidal currents inhibit the development of density stratification and minimize any longitudinal density gradient that might otherwise exist between the Outer Lagoon and the shallow Entrance Channel (cf. Largier et al., 1997; Winant and Gutiérrez de Velasco, 2003; Kämpf and Ellis, 2015).

5. Discussion

Sedimentation in the Khor Al Adaid is strongly influenced by its setting in a hot, hyper-arid climate zone, some of the effects being obvious, but others less so. Most obviously, the hyper-arid setting means that there is little or no rainfall, which has a dramatic impact on the nature of the supply of siliciclastic sediment to the system: there is no river input so that eolian supply, coupled with in situ carbonate production, dominates. The dominance of eolian input means that the sediment within most of the system consists mainly of sand-sized material that has a relatively narrow grain-size distribution. Terrigenous-clastic mud is conspicuously scarce because of the lack of river input, the only source of such fine-grained siliciclastic material being wind-blown dust. The absence of this fine material has several implications. First, as noted earlier, the dominance of non-cohesive sediment has determined the shape of the flood-tidal deltas, causing them to have lobate forms instead of a more birdsfoot morphology. Second, the material that would normally accumulate in the upper part of the intertidal zone is scarce; its absence means that this depositional environment is not well represented in the deposits of this embayment. Instead, on FTD 1, sandy deposits that now lie in the upper intertidal zone are believed to have been stranded there as a result of a small, relative sea-level fall, and have not been buried by muddy deposits. In places where the gradient of the shoreline is very gentle and the full gradation of intertidal environments exist, the upper intertidal zone is occupied by extensive microbial mats of various forms rather than by muddy deposits. Finally, the absence of siliciclastic mud means that the water is generally very clear. Not only does this allow detailed determination of the bathymetry from satellite images, but it also allows greater penetration of light and an expanded photic zone relative to muddy estuarine systems. This promotes the broader distribution of microbial and algal communities, and also of organisms with photosymbionts (e.g., the corals that formerly lived in the outer part of the system).

The lack of fresh-water input allows salinities to become elevated, which promotes the development of extensive microbial mats and, ultimately, the precipitation of gypsum in the sediment. The longitudinal gradient of salinities from the mouth to the head of the system is reflected in the pattern of faunal diversity, and the particular types of organisms present in each sector of the system. A more subtle but no less important impact of the lack of fresh-water input is the overwhelming flood-tide dominance of sediment transport. In tide-dominated estuaries (sensu Dalrymple et al., 1992, 2012), the main thalweg is typically ebb-dominant, with flood-dominant areas occurring in flanking positions in the form of headward-terminating flood barbs. Thus, the morphology seen in the Entrance Channel is unusual, with a throughgoing flood-dominant thalweg that is flanked by seaward-terminating "ebb barbs". In the Khor Al Adaid, however, there is no river discharge to augment the ebb tide, thereby allowing an accentuated flood-tide dominance.

The relatively few studies that have been done on flow within inverse estuaries have found that the longitudinal density gradient is rarely strong enough to generate significant seaward-directed flow.

The gradient is strongest in the inner part of the system (Vethamony et al., 2007; Kämpf and Ellis, 2015) where the tidal mixing is least, as is the case in the Khor Al Adaid (Fig. 9). However, this gradient is counterbalanced by friction because this area is generally shallow, a factor that makes inverse circulation less likely (Largier et al., 1997). Further seaward, stronger tidal currents cause more effective mixing, thereby decreasing the longitudinal density gradient and further minimizing the potential for the development of inverse estuarine circulation. In addition to this, it is common in such estuaries for the water near the head to be warmer (i.e., lighter) than the water in the open-marine area, a trend that acts against the seaward-directed density gradient due to salinity. In some systems, the two gradients effectively cancel each other (Postma, 1965; Winant and Gutiérrez de Velasco, 2003; Largier, 2010). The conclusion appears to be that inverse estuarine circulation will be weak, if it exists at all, and is, therefore, unlikely to play a significant role in the transport of sand in arid-zone estuaries, although it might be more important in the transport of fine-grained suspended sediment (Postma, 1965). More work is needed to confirm these conclusions.

The presence of the large eolian dunes in the area surrounding the Inner Lagoon has a direct influence on the shape of this water body. The almost complete isolation of sub-basins by the presence of these large bedforms increases the restriction that these areas experience, and could increase the potential to develop evaporites in these areas. This morphological control on system morphology by the dunes would probably have been more extensive if it wasn't for the influence exerted by faulting and karst collapse in the outer sectors of the embayment.

The Khor Al Adaid is unlike any other coastal system described in detail so far, but it is thought to be representative of a particular type of eolian-marine interaction. Specifically, it must be noted that many of the characteristics of this system exist because the winds are blowing in an offshore direction, thereby carrying sand into the coastal zone rather than away from it as is the case in the nearby coast of the United Arab Emirates (i.e., the so-called Trucial Coast) where the winds blow onshore. As noted by Fryberger et al. (1983), areas with offshore-directed winds will tend to have coasts dominated by siliciclastic sediment, whereas coasts with onshore winds will generally have carbonate-dominated coastal zones. This is clearly the case in Qatar, where the northern and eastern coasts that experience onshore winds are generally fringed by carbonate sediments (Wagner and van der Togt, 1973; Billeaud et al., 2014; Purkis et al., 2017; Rivers et al., 2019b), whereas the south-eastern coast with its offshore winds is composed dominantly of siliciclastic sand (Shinn, 1973; this study).

The presence of offshore-directed winds also means that the shoreline is a lee coast with respect to locally generated waves and, therefore, is likely to have low wave energy. This is especially the case in the Khor Al Adaid where the complex geometry and small scale of the lagoons means that dunes migrating into the sea are not significantly modified by wave action (cf. Fig. 18H in Rodríguez-López et al. (2012)). Beaches are not significant in this setting (Shinn, 1973; Billeaud et al., 2014), and those in protected areas such as the Inner Lagoon have characteristics that are transitional into microbially bound tidal flats. The general lack of wave reworking and significant erosion during transgression creates a complex coastal morphology, as the water floods in amongst the dunes, creating conditions favorable for the development of significant water restriction, as is the case in the Inner Lagoon of the Khor Al Adaid. By contrasted, coasts with high wave energy are likely to show less complex sedimentation patterns, because wave energy will straighten the coast, and ravinement will cut more deeply. An example is provide by the coast of northern Mauritania, that, despite being a lee coast (Sarnthein and Diester-Haass, 1977; Barusseau et al., 2010; Hanebuth et al., 2013), exposed to intense wave action because of exposure to the open Atlantic Ocean. There, the coast has a well-developed beach and shoreface with no morphological expression of the advance of eolian dunes into the surf zone. In this situation, progradation of the coast is caused by the arrival of dunes, but the deposits of the coastal platform will be marine in origin, unlike the low-energy coast that occurs in the Khor Al Adaid and the adjacent coast to the north (Shinn, 1973).

The (partial) preservation of eolian topographic relief during transgressions has been the subject of considerable interest over the years, mainly because of the potential for this relief to act as stratigraphic hydrocarbon traps (Glennie and Buller, 1983; Huntoon and Chan, 1987; Chan, 1989; Jones and Blakey, 1993; Kamola and Huntoon, 1994; Ahmed Benan and Kocurek, 2000). The wave energy at the shoreline is clearly a first-order control on the extent to which dunes survive passage through the beach and shoreface during transgression, with the potential to preserve a greater fraction of the dune relief increasing as the wave energy and the depth of ravinement decrease. Thus, partial dune preservation is likely to be greater in low-energy areas such as the eastern coast of Qatar than along the Mauritanian shoreline. The Khor Al Adaid illustrates a different control on the preservation of eolian topopgraphy. Here, the dunes surrounding the Inner Lagoon are at the trailing edge of the dune field, so that additional sand is not being added to replace the material deposited in the lagoons. Thus, the superstructure of the draa is being deflated so that only the lower part of the bedform exists at the time when marine waters flood the interdune areas.

6. Conclusions

The Khor Al Adaid tidal embayment in southeastern Qatar provides a modern analogue for eolian-marine interaction in areas where the wind and dunes move in an offshore direction, feeding sand into a low-energy coastal zone. It consists of three main sectors: the relatively straight Entrance Channel, the orientation and width of which are likely controlled by faulting; the ovoid Outer Lagoon, which may occupy a karst-collapse structure; and the irregularly shaped Inner Lagoon that occupies the interdune areas between the deflated roots of several large eolian bedforms. Tidal currents dominate sedimentation in all narrow constrictions, including the Entrance Channel and the entrances to the Inner Lagoon and the small sub-basin that lies to its east. Locally generated wind waves influence sedimentation in the open water of the lagoons and locally generate beaches at the high-tide level. The system is strongly flood-tide dominant, such that the sand that is dumped into the northern margin of the various water bodies is transferred landward to form a series of three flood-tide deltas, one in the Outer Lagoon, and two in the Inner Lagoon—one at its mouth, and another on the landward side of a narrow passage through one of the confining eolian bedforms. The morphology of the sand accumulations in the Entrance Channel, and particularly the presence of a through-going flood-dominant thalweg that is flanked by seaward-terminating “ebb barbs”, suggests that the flood-tide dominance is stronger than it is normally the case in coastal embayments, perhaps because of the absence of any river discharge to accentuate the ebb-tidal currents. The apparent absence of inverse estuarine circulation with seaward flow of more saline water at the bed, which might have accentuated any ebb currents, is attributed to the great depth of the Outer Lagoon, which traps the dense brine that does flow seaward from the Inner Lagoon, coupled with intense tidal mixing in the shallow Entrance Channel. Almost the only siliciclastic sediment entering the system is sand that is supplied along the entire northern margin of the system by eolian dunes, generating large-scale cross beds that interfinger with channel and lagoonal deposits; siliciclastic mud is essentially absent, except for a very minor component of eolian dust. As a result, most of the deposits consist of nearly pure quartz-rich sand. The absence of siliciclastic mud inhibits the formation of upper-intertidal deposits and causes the flood-tidal deltas to have a pronounced lobate geometry, as has been shown to be the case for river-dominated fluvial deltas formed predominantly of sand. The low-energy central portions of the lagoons are floored by carbonate mud produced locally. Gypsum is precipitating in the most

restricted part of the Inner Lagoon. The benthic fauna contributes a minor component of the sediment; the diversity and types of benthic organisms present reflect the landward increase in salinity. The partial preservation of relief on the large eolian dunes is favored by the low-energy, lee-coast setting. In the Inner Lagoon area, much of the eolian relief has been removed by deflation, with transfer of the sediment into the lagoon, because the dunes represent the trailing edge of the dune field. Because this is the first detailed sedimentological description of an arid-zone coastal embayment that we know of, many aspects of its morphodynamics and facies remain to be documented fully Additional studies of such environments are needed.

Declaration of competing interest

The authors declare that they have no known competing financial interests or personal relationships that could have appeared to influence the work reported in this paper.

Acknowledgements

This work is dedicated to the late Professor Mohamed Alaa Abdel-Moati, Environmental Consultant for the Qatar Ministry of Municipality & Environment. Dr. Abdel-Moati unfailingly supported work dedicated to increasing the understanding of Qatar's natural systems. Great appreciation is also extended to Saleh Al Kuwari and personnel of the Qatar Ministry for Municipality and Environment, without whose logistical support and provision of sea craft this study could not have been completed. JMR is indebted to Christian Strohmenger for introducing him to the study area and providing advice on the morphological terms used for microbial-mat descriptions. The authors appreciate Sarah Vest for her aid in referencing and proofing the manuscript. We are grateful to Venkat Kolluru and his team for assisting in building the computer-based physical oceanographic model. Helpful reviews of the manuscript were provided by Brian Pratt and an anonymous reviewer.

References

Adenekan, A.E., Kolluru, V.S., Smith, J.P., 2009. Transport and fate of chlorinated by-products associated with cooling water discharges. In: Alfadala, G.V., Reklaitis, R., El-Halwagi, M.M. (Eds.), Proceedings of the 1st Annual Gas Processing Symposium. 27 July 2009. Elsevier, pp. 341–353.

Ahmed Benan, C.A., Kocurek, G., 2000. Catastrophic flooding of an aeolian dune field: Jurassic Entrada and Todilto formations, Ghost Ranch, New Mexico, USA. Sedimentology 47, 1069–1080.

Al Mamoon, A., Joergensen, N.E., Rahman, A., Qasem, H., 2014. Derivation of new design rainfall in Qatar using L-moment based index frequency approach. Int. J. Sustain. Built Environ. 3, 111–118.

Al-Khayat, J.A., Al-Mohannadi, M.S., 2006. Ecology and biology of the benthic bivalve *Aminatis umbonella* (Lamark) in Khor Al Adaid, Qatar. Egypt. J. Aquat. Res. 32, 419–430.

Al-Yousef, M., 2003. Mineralogy, Geochemistry and Origin of Quaternary Sabkhas in the Qatar Peninsula, Arabian Gulf. (Unpublished thesis). University of Southhapton, UK.

Ashley, G.M., 1990. Classification of large-scale subaqueous bedforms; a new look at an old problem. J. Sediment. Res. 60, 160–172.

Ashour, M., 1987. Surficial Deposits of Qatar Peninsula. Desert Sediments: Ancient and Modern. 35. Geological Society, London, Special Publications 361–367 pp.

Barusseau, J., Certain, R., Vernet, R., Saliège, J., 2010. Late Holocene morphodynamics in the littoral zone of the Iwik Peninsula area (Banc d'Arguin—Mauritania). Geomorphology 121, 358–369.

Bhattacharya, J.P., 2010. Deltas. In: James, N., Dalrymple, R.W. (Eds.), Facies Models 4. Geological Association of Canada, pp. 233–264.

Billeaud, I., Caline, B., Livas, B., Tessier, B., Davaud, E., Frebourg, G., Hasler, C.-A., Laurier, D., Pabian-Goyheneche, C., 2014. The carbonate-evaporite lagoon of Al Dakhirah (Qatar): an example of a modern depositional model controlled by longshore transport. In: Martini, I.P., Wanless, H.R. (Eds.), Sedimentary Coastal Zones from High to Low Latitiudes: Similarities and Differences. London, Special Publications, Geological Society, pp. 561–587.

Blakey, R.C., Havholm, K.G., Jones, L.S., 1996. Stratigraphic analysis of eolian interactions with marine and fluvial deposits, Middle Jurassic Page Sandstone and Carmel Formation, Colorado Plateau, USA. J. Sediment. Res. 66, 324–342.

Blanchard, S., Fielding, C.R., Frank, T.D., Barrick, J.E., 2016. Sequence stratigraphic framework for mixed aeolian, peritidal and marine environments: Insights from the Pennsylvanian subtropical record of Western Pangaea. Sedimentology 63, 1929–1970.

Burpee, A.P., Slingerland, R.L., Edmonds, D.A., Parsons, D., Best, J., Cederberg, J., McGuffin, A., Caldwell, R., Nijhuis, A., Royce, J., 2015. Grain-size controls on the morphology and internal geometry of river-dominated deltas. J. Sediment. Res. 85, 699–714.

Cacchione, D.A., Drake, D.E., Grant, W.D., Tate, G.B., 1984. Rippled scour depressions on the inner continental shelf off central California. J. Sediment. Res. 54, 1280–1291.

Caldwell, R.L., Edmonds, D.A., 2014. The effects of sediment properties on deltaic processes and morphologies: a numerical modeling study. J. Geophys. Res. Earth Surf. 119, 961–982.

Chan, M.A., 1989. Erg margin of the Permian White Rim Sandstone, SE Utah. Sedimentology 36, 235–251.

Ciftci, B., Aviantara, A., Hurley, N., Kerr, D., 2004. Outcrop-based three-dimensional modeling of the Tensleep sandstone at Alkali Creek, Bighorn Basin, Wyoming. In: Grammar, G.M., Harris, P.M., Eberli, G.P. (Eds.), Integration of Outcrop and Modern Analogs in Reservoir Modeling. AAPG, pp. 235–259.

Clarke, M.H., Keij, A., 1973. Organisms as producers of carbonate sediment and indicators of environment in the southern Persian Gulf. In: Purser, B.H. (Ed.), The Persian Gulf. Springer, Berlin, Heidelberg, pp. 33–56.

Dalrymple, R.W., 2010. Tidal depositional systems. In: James, N.P., Dalrymple, R.W. (Eds.), Facies Models 4. Geological Association of Canada, St. John's, Newfoundland, Canada, pp. 201–231.

Dalrymple, R., Choi, K., 2003. Sediment transport by tides. In: Middleton, G.V. (Ed.), Encyclopedia of Sediments and Sedimentary Rocks. Springer, Dordrecht, pp. 606–609.

Dalrymple, R.W., Rhodes, R.N., 1995. Estuarine dunes and bars. In: Perillo, G.M.E. (Ed.), Developments in Sedimentology. Elsevier, pp. 359–422.

Dalrymple, R.W., Zaitlin, B.A., Boyd, R., 1992. Estuarine facies models; conceptual basis and stratigraphic implications. J. Sediment. Res. 62, 1130–1146.

Dalrymple, R.W., Mackay, D.A., Ichaso, A.A., Choi, K.S., 2012. Processes, morphodynamics, and facies of tide-dominated estuaries. In: Davis Jr., R.A., Dalrymple, R.W. (Eds.), Principles of Tidal Sedimentology. Springer, Dordrecht, pp. 79–107.

Davidson-Arnott, R., 2013. Nearshore bars. In: Shroder, J., Sherman, D.J. (Eds.), Treatise on Geomorphology. Academic Press, San Diego, CA, pp. 130–148.

Dawson, J.C., Davidson-Arnott, R.G., Ollerhead, J., 2002. Low-energy morphodynamics of a ridge and runnel system. J. Coast. Res. 36, 198–215.

Doornkamp, J.C., Brunsden, D., Jones, D.K., 1980. Geology, Geomorphology and Pedology of Bahrain. University of East Anglia, Geo Abstracts Ltd., Norwich, UK.

Eccleston, B., Pike, J., Harhash, I., 1981. The Water Resources of Qatar and Their Development. Ministry of Industry and Agriculture Doha.

Edmonds, D.A., Slingerland, R.L., 2010. Significant effect of sediment cohesion on delta morphology. Nat. Geosci. 3, 105–109.

Elshorbagy, W., Azam, M.H., Taguchi, K., 2006. Hydrodynamic characterization and modeling of the Arabian Gulf. J. Waterw. Port Coast. Ocean Eng. 132, 47–56.

Embabi, N.S., Ashour, M.M., 1993. Barchan dunes in Qatar. J. Arid Environ. 25, 49–69.

Engel, M., Brückner, H., 2014. The South Qatar Survey Project (SQSP)–preliminary findings on Holocene coastal changes and geoarchaeological archives. Zeitschrift für Orient-Archäologie. 7, pp. 290–301.

Engel, M., Ruckmann, S., Drechsler, P., Brill, D., Opitz, S., Fassbinder, J.W., Pint, A., Peis, K., Wolf, D., Gerber, C., Pfeiffer, K., Eichmann, R., Bruckner, H., 2020. Sediment-filled karst depression and *riyad* - Key archaelogical environments of South Qatar. E&G Quat. Sci. J. 68, 215–236.

ERM, 2006. A User Guide to Customize GEMSS Computations. Exton, PA.

Eschner, T.B., Kocurek, G., 1988. Origins of relief along contacts between eolian sandstones and overlying marine strata. AAPG Bull. 72, 932–943.

Eugenio, F., Marcello, J., Martin, J., 2015. High-resolution maps of bathymetry and benthic habitats in shallow-water environments using multispectral remote sensing imagery. IEEE Trans. Geosci. Remote Sens. 53, 3539–3549.

Fairbridge, R.W., 1961. Eustatic changes in sea level. Phys. Chem. Earth 4, 99–185.

Falqués, A., Dodd, N., Garnier, R., Ribas, F., Machardy, L.C., Larroudé, P., Calvete, D., Sancho, F., 2008. Rhythmic surf zone bars and morphodynamic self-organization. Coast. Eng. 55, 622–641.

Febbo, E., Kolluru, V., Prakash, S., Adenekan, A., 2012. Numerical Modeling of Thermal Plume and Residual Chlorine Fate in Coastal Waters of the Arabian Gulf. SPE-156813-PP. Presented at the SPE/APPEA International Conference on Health, Safety, and Environment in Oil and Gas Exploration and Production, Perth, Western Australia, pp. 11–13 September 2012.

Ferrini, V.L., Flood, R.D., 2005. A comparison of Rippled Scour Depressions identified with multibeam sonar: evidence of sediment transport in inner shelf environments. Cont. Shelf Res. 25, 1979–1995.

Fryberger, S.G., Al-Sari, A.M., Clisham, T.J., 1983. Eolian dune, interdune, sand sheet, and siliciclastic sabkha sediments of an offshore prograding sand sea, Dhahran area, Saudi Arabia. AAPG Bull. 67, 280–312.

Fryberger, S.G., Krystinik, L.F., Schenk, C.J., 1990. Tidally flooded back-barrier dunefield, Guerrero Negro area, Baja California, Mexico. Sedimentology 37, 23–43.

Garnaud, S., Lesueur, P., Garlan, T., 2005. Origin of rippled scour depressions associated with cohesive sediments in a shoreface setting (eastern Bay of Seine, France). Geo-Mar. Lett. 25, 34–42.

Garnier, R., Calvete, D., Falqués, A., Calalleria, M., 2006. Generation and nonlinear evolution of shore-oblique/transverse sand bars. J. Fluid Mech. 567, 327–360.

Garzanti, E., Vermeesch, P., Andò, S., Vezzoli, G., Valagussa, M., Allen, K., Kadi, K.A., Al-Juboury, A.I., 2013. Provenance and recycling of Arabian desert sand. Earth Sci. Rev. 120, 1–19.

Glennie, K.W., 2005. The Desert of Southeast Arabia: Desert Environments and Sediments (Gulf PetroLink).

Glennie, K., Buller, A., 1983. The Permian Weissliegend of NW Europe: the partial deformation of aeolian dune sands caused by the Zechstein transgression. Sediment. Geol. 35, 43–81.

Hanebuth, T.J., Mersmeyer, H., Kudrass, H.-R., Westphal, H., 2013. Aeolian to shallow-marine shelf architecture off a major desert since the Late Pleistocene (northern Mauritania). Geomorphology 203 (Supplementary Special Issue: Continental Shelf Drowned Landscapes (INQUA-CMP and IGCP-526)), 132–147.
Healy, T., Wang, Y., Healy, J.A., Augustinus, P., Baba, M., Bao, C., Flemming, B., Fortes, M., Han, M., Marone, E., Mehta, A., Ke, X., Kirby, R., Kjerfve, B., Schaeffer-Novelli, Y., Wolanski, E., 2002. Definition, properties, and classification of muddy coasts. In: Healy, H.T., Wang, R.Y., Healy, J.A. (Eds.), Muddy Coasts of the World: Processes, Deposits, and Function, p. 9.
Houbolt, J.J.H.C., 1957. Surface Sediments of the Persian Gulf near the Qatar Peninsula. Mouton, The Hauge.
Howari, F.M., Aldouri, R., Sadiq, A., 2016. Gravity investigations of recent sinkholes and karst pits of Dahal Al-Hamam, State of Qatar. Environ. Earth Sci. 75, 440.
Hoyal, D.C.J.D., Sheets, B.A., 2009. Morphodynamic evolution of experimental cohesive deltas. J. Geophys. Res. Earth Surf. 114, 18.
Hunter, J.R., 1983. Aspects of the dynamics of the residual circulation of the Arabian Gulf. In: Gade, H.G., Edwards, A., Svendsen, H. (Eds.), Coastal Oceanography. NATO Conference Series. Springer, Boston, MA, pp. 31–42.
Huntoon, J.E., Chan, M.A., 1987. Marine origin of paleotopographic relief on eolian White Rim Sandstone (Permian), Elaterite basin, Utah. AAPG Bull. 71, 1035–1045.
Javed, W., Wubulikasimu, Y., Figgis, B., Guo, B., 2017. Characterization of dust accumulated on photovoltaic panels in Doha, Qatar. Sol. Energy 142, 123–135.
Jenkins, A.D., 1987. Wind and wave induced currents in a rotating sea with depth-varying eddy viscosity. J. Phys. Oceanogr. 17, 938–951.
Jones, L.S., Blakey, R.C., 1993. Erosional remnants and adjacent unconformities along an eolian-marine boundary of the Page Sandstone and Carmel Formation, Middle Jurassic, south-central Utah. J. Sediment. Res. 63, 852–859.
Jordan, O.D., Mountney, N.P., 2010. Styles of interaction between aeolian, fluvial and shallow marine environments in the Pennsylvanian to Permian lower Cutler beds, southeast Utah, USA. Sedimentology 57, 1357–1385.
Jordan, O.D., Mountney, N.P., 2012. Sequence stratigraphic evolution and cyclicity of an ancient coastal desert system: the Pennsylvanian–Permian Lower Cutler Beds, Paradox Basin, Utah, USA. J. Sediment. Res. 82, 755–780.
Kamola, D.L., Chan, M.A., 1988. Coastal dune facies, Permian Cutler Formation (White Rim Sandstone), Capitol Reef National Park area, southern Utah. Sediment. Geol. 56, 341–356.
Kamola, D.L., Huntoon, J.E., 1994. Changes in rate of transgression across the Permian White Rim Sandstone, southern Utah. J. Sediment. Res. 64, 202–210.
Kämpf, J., Ellis, H., 2015. Hydrodynamics and flushing of Coffin Bay, South Australia: a small tidal inverse estuary of interconnected bays. J. Coast. Res. 31, 447–456.
Karl, H.A., 1980. Speculations on processes responsible for mesoscale current lineations on the continental shelf, southern California. Mar. Geol. 34, M9–M18.
Kassler, P., 1973. The structural and geomorphic evolution of the Persian Gulf. In: Purser, B.H. (Ed.), The Persian Gulf. Springer, Berlin, Heidelberg, pp. 11–32.
Kenyon, N.H., 1970. Sand ribbons of European tidal seas. Mar. Geol. 9, 25–39.
Kerr, D.R., Dott Jr., R.H., 1988. Eolian dune types preserved in the Tensleep Sandstone (Pennsylvanian-Permian), north-Central Wyoming. Sediment. Geol. 56, 383–402.
Kocurek, G., 1988. First-order and super bounding surfaces in eolian sequences—bounding surfaces revisited. Sediment. Geol. 56, 193–206.
Kolluru, V.S., Buchak, E.M., Edinger, J.E., Brinkmann, P.E., 2002. Three-Dimensional thermal modeling of the rasgas cooling water outfall. In: Spaulding, M.L. (Ed.), 7th International Conference on Estuarine and Coastal Modeling (2001). American Society of Civil Engineers, St. Petersberg, FL, pp. 893–912.
Konicki, K.M., Holman, R.A., 2000. The statistics and kinematics of transverse sand bars on an open coast. Mar. Geol. 169, 69–101.
Lambeck, K., 1996. Shoreline reconstructions for the Persian Gulf since the last glacial maximum. Earth Planet. Sci. Lett. 142, 43–57.
Lardner, R., Lehr, W., Fraga, R., Sarhan, M., 1988. A model of residual currents and pollutant transport in the Arabian Gulf. Appl. Math. Model. 12, 379–390.
Largier, J., 2010. Low-inflow estuaries: hypersaline, inverse and thermal scenarios. In: Valle-Levinson, A. (Ed.), Contemporary Issues in Estuarine Physics. Cambridge University Press, pp. 247–272.
Largier, J., Hollibaugh, J.T., Smith, S., 1997. Seasonally hypersaline estuaries in Mediterranean-climate regions. Estuar. Coast. Shelf Sci. 45, 789–797.
Legleiter, C., Tedesco, M., Smith, L., Behar, A., Overstreet, B., 2014. Mapping the bathymetry of supraglacial lakes and streams on the Greenland Ice Sheet using field measurements and high resolution satellite images. Cryosphere 8, 215–228.
Leon, J.G., Calmant, S., Seyler, F., Bonnet, M.-P., Cauhopé, M., Frappart, F., Filizola, N., Fraizy, P., 2006. Rating curves and estimation of average water depth at the upper Negro River based on satellite altimeter data and modeled discharges. J. Hydrol. 328, 481–496.
Lokier, S.W., Knaf, A., Kimiagar, S., 2013. A quantitative analysis of recent arid coastal sedimentary facies from the Arabian Gulf Coastline of Abu Dhabi, United Arab Emirates. Mar. Geol. 346, 141–152.
Loreau, J.-P., Purser, B., 1973. Distribution and ultrastructure of Holocene ooids in the Persian Gulf. In: Purser, B.H. (Ed.), The Persian Gulf. Springer, Berlin, Heidelberg, pp. 279–328.
Loughland, R.A., Al-Abdulkader, K.A., Wyllie, A., Burwell, B.O., 2012. Anthropogenic induced geomorphological change along the Western Arabian Gulf coast. In: Piacentini, T., Miccadei, E. (Eds.), Studies on Environmental and Applied Geomorphology. InTech Open Access Publisher.
Mariño, J.E., Morris, T.H., 1996. Erg margin and marginal marine facies analysis of the Entrada Sandstone, Utah: implications to depositional models and hydrocarbon entrapment. The Continental Jurassic: Museum of Northern Arizona Bulletin. 60, pp. 483–496.
Maritorena, S., Morel, A., Gentili, B., 1994. Diffuse reflectance of oceanic shallow waters: Influence of water depth and bottom albedo. Limnol. Oceanogr. 39, 1689–1703.
McLean, S.R., 1981. The role of non-uniform roughness in the formation of sand ribbons. In: Nittrouer, C.A. (Ed.), Sedimentary Dynamics of Continental Shelves Developments in Sedimentology. Elsevier, pp. 49–74.
Medellin, G., Medina, R., Falqués, A., González, M., 2008. Coastline sand waves on a low-energy beach at "El Puntal" spit, Spain. Mar. Geol. 250, 143–156.
Mitrovica, J., Milne, G., 2002. On the origin of late Holocene sea-level highstands within equatorial ocean basins. Quat. Sci. Rev. 21, 2179–2190.
Murty, T.S., El-Sabh, M.I., 1989. Storm tracks, storm surges and sea state in the Arabian Gulf, Strait of Hormuz and the Gulf of Oman. In: El-Sabh, M.I. (Ed.), Oceanographic Modelling of the Kuwait Action Plan (KAP) Region. UNESCO Reports in Marine Science, No. 28, pp. 12–24.
Paulo, C., Dittrich, M., 2013. 2D Raman spectroscopy study of dolomite and cyanobacterial extracellular polymeric substances from Khor Al-Adaid sabkha (Qatar). J. Raman Spectrosc. 44, 1563–1569.
Pope, A., Scambos, T.A., Moussavi, M., Tedesco, M., Willis, M., Shean, D., Grigsby, S., 2016. Estimating supraglacial lake depth in West Greenland using Landsat 8 and comparison with other multispectral methods. Cryosphere 10, 15–27.
Postma, H., 1965. Water circulation and suspended matter in Baja California lagoons. Neth. J. Sea Res. 2, 566–604.
Pous, S., Carton, X.J., Lazure, P., 2012. A process study of the tidal circulation in the Persian Gulf. Open J. Mar. Sci. 2, 131–140 Scientific Research Publishing.
Pous, S., Carton, X.J., Lazure, P., 2013. A process study of the wind-induced circulation in the Persian Gulf. Open J. Mar. Sci. 3, 1–11 Scientific Research Publishing.
Prakash, S., Kolluru, V.S., 2014. Implementation of integrated modelling approach to impact assessment applications for LNG operations using 3-D comprehensive modelling framework. 7th International Congress on Environmental Modelling and Software. International Environmental Modelling & Software Society, Provo, Utah, pp. 556–564 15-19 June 2014, San Diego, California.
Pritchard, D.W., 1955. Estuarine Circulation Pattern. Proc. Am. Soc. Civ. Eng. 81, 1–11.
Purkis, S., Rivers, J., Strohmenger, C.J., Warren, C., Yousif, R., Ramirez, L., Riegl, B., 2017. Complex interplay between depositional and petrophysical environments in Holocene tidal carbonates (Al Ruwais, Qatar). Sedimentology 64, 1646–1675.
Purser, B.H., Evans, G., 1973. Regional Sedimentation along the Trucial Coast, SE Persian Gulf, the Persian Gulf. Springer, Berlin, Heidelberg, pp. 211–231.
Purser, B.H., Loreau, J.-P., 1973. Aragonitic, supratidal encrustations on the Trucial coast, Persian Gulf. In: Purser, B.H. (Ed.), The Persian Gulf. Springer, Berlin, Heidelberg, pp. 343–376.
Reimer, P.J., Bard, E., Bayliss, A., Beck, J.W., Blackwell, P.G., Bronk Ramsey, C., Buck, C.E., Cheng, H., Edwards, R.L., Friedrich, M., Grootes, P.M., Guilderson, T.P., Haflidason, H., Hajdas, I., Hatté, C., Heaton, T.J., Hoffmann, D.L., Hogg, A.G., Hughen, K.A., Kaiser, K.F., Kromer, B., Manning, S.W., Niu, M., Reimer, R.W., Richards, D.A., Scott, E.M., Southon, J.R., Staff, R.A., Turney, C.S.M., van der Plicht, J., 2013. IntCal13 and Marine13 radiocarbon age calibration curves 0–50,000 years cal BP. Radiocarbon 55, 1869–1887.
Rezaei-Latifi, A., 2016. Spatial and temporal variability of the surface permittivity of Persian Gulf water at the C-band. Appl. Math. Model. 40, 1069–1081.
Ribas, F., Falqués, A., Garnier, R., 2017. Nearshore sand bars. Chapter 13. In: Guillés, J., Acosta, J., Chiocci, F.L., Palanques, A. (Eds.), Atlas of Bedforms in the Western Mediterranean. Springer International Publishing, Cham, Switzerland, pp. 73–79 Chapter 13.
Ridd, P., Stieglitz, T., 2002. Dry season salinity changes in arid estuaries fringed by mangroves and saltflats. Estuar. Coast. Shelf Sci. 54, 1039–1049.
Rivers, J.M., Larson, K.P., 2018. The Cenozoic kinematics of Qatar: evidence for high-angle faulting along the Dukhan 'anticline'. Mar. Pet. Geol. 92, 953–961.
Rivers, J.M., Varghese, L., Yousif, R., Whitaker, F.F., Skeat, S.L., Al-Shaikh, I., 2019a. The geochemistry of Qatar coastal waters and its impact on carbonate sediment chemistry and early marine diagenesis. J. Sediment. Res. 89, 293–309.
Rivers, J.M., Engel, M., Dalrymple, R., Yousif, R., Strohmenger, C.J., Al-Shaikh, I., 2019b. Are carbonate barrier islands mobile? Insights from a mid to late-Holocene system, Al Ruwais, northern Qatar. Sedimentology 67, 534–538.
Robinson, A.H.W., 1960. Ebb-flood channel systems in sandy bays and estuaries. Geography 45, 183–199.
Rodríguez-López, J.P., Melendez, N., De Boer, P.L., Soria, A.R., 2008. Aeolian sand sea development along the mid-Cretaceous western Tethyan margin (Spain): erg sedimentology and palaeoclimate implications. Sedimentology 55, 1253–1292.
Rodríguez-López, J.P., Melendez, N., De Boer, P.L., Soria, A.R., 2012. Controls on marine–erg margin cycle variability: aeolian–marine interaction in the mid-Cretaceous Iberian Desert System, Spain. Sedimentology 59, 466–501.
Sadrinasab, M., Kenarkohi, K., 2009. Three-dimensional numerical modelling study of sound speed in the Persian Gulf. Asian J. Appl. Sci. 2, 232–239.
Sarnthein, M., 1972. Sediments and history of the postglacial transgression in the Persian Gulf and northwest Gulf of Oman. Mar. Geol. 12, 245–266.
Sarnthein, M., Diester-Haass, L., 1977. Eolian-sand turbidites. J. Sediment. Res. 47, 868–890.
Sarnthein, M., Walger, E., 1974. Der äolische sandstrom aus der W-Sahara zur Atlantikküste. Geol. Rundsch. 63, 1065–1987.
Seltrust Engineering, Limited, 1980. Qatar Geological Map Explanatory Booklet. Doha, Qatar.
Shinn, E.A., 1973. Sedimentary accretion along the leeward, SE coast of Qatar Peninsula, Persian Gulf. In: Purser, B.H. (Ed.), The Persian Gulf. Springer, Berlin, Heidelberg, pp. 199–209.
Shinn, E.A., Steinen, R.P., Lidz, B.H., Swart, P.K., 1989. Whitings, a sedimentologic dilemma. J. Sediment. Petrol. 59 (1), 147–161.
Southon, J., Kashgarian, M., Fontugne, M., Metivier, B., Yim, W.W., 2002. Marine reservoir corrections for the Indian Ocean and Southeast Asia. Radiocarbon 44, 167–180.

Stern, R.J., Johnson, P., 2010. Continental lithosphere of the Arabian Plate: a geologic, petrologic, and geophysical synthesis. Earth Sci. Rev. 101, 29–67.
Stokes, W.L., 1968. Multiple parallel-truncation bedding planes; a feature of wind-deposited sandstone formations. J. Sediment. Res. 38, 510–515.
Straub, K.M., Paola, C., Mohrig, D., Wolinsky, M.A., George, T., 2009. Compensational stacking of channelized sedimentary deposits. J. Sediment. Res. 79, 673–688.
Strohmenger, C.J., Jameson, J., 2015. Modern coastal systems of Qatar as analogues for arid climate carbonate reservoirs: improving geological and reservoir modelling. First Break 33, 41–50.
Stumpf, R.P., Holderied, K., Sinclair, M., 2003. Determination of water depth with high-resolution satellite imagery over variable bottom types. Limnol. Oceanogr. 48, 547–556.
Vahtmäe, E., Kutser, T., 2007. Mapping bottom type and water depth in shallow coastal waters with satellite remote sensing. J. Coast. Res. 185–189.
Van Den Berg, N., Falqués, A., Ribas, F., Caballeria, M., 2014. On the mechanism of wavelength selection of self-organized shoreline sand waves. J. Geophys. Res. Earth Surf. 119, 665–681.
Vaselali, A., Vaselali, M., 2009. Modelling of brine waste discharges spreading under tidal currents. J. Appl. Sci. 9, 3454–3468.
Vethamony, P., Babu, M., Ramanamurty, M., Saran, A., Joseph, A., Sudheesh, K., Padgaonkar, R.S., Jayakumar, S., 2007. Thermohaline structure of an Inverse Estuary–the Gulf of Kachchh: Measurements and model simulations. Mar. Pollut. Bull. 54, 697–707.
Wagner, C., Van der Togt, C., 1973. Holocene sediment types and their distribution in the southern Persian Gulf. In: Purser, B.H. (Ed.), The Persian Gulf. Springer, Berlin, Heidelberg, pp. 123–155.
Wang, P., 2012. Principles of sediment transport applicable in tidal environments. In: Davis Jr., R.A., Dalrymple, R.W. (Eds.), Principles of Tidal Sedimentology. Springer, Dordrecht, pp. 19–34.
Wang, Y., Straub, K.M., Hajek, E.A., 2011. Scale-dependent compensational stacking: an estimate of autogenic time scales in channelized sedimentary deposits. Geology 39, 811–814.
Warren, C., Dupont, J., Abdel-Moati, M., Hobeichi, S., Palandro, D., Purkis, S., 2016. Remote sensing of Qatar nearshore habitats with perspectives for coastal management. Mar. Pollut. Bull. 105, 641–653.
Winant, C.D., Gutiérrez de Velasco, G., 2003. Tidal dynamics and residual circulation in a well-mixed inverse estuary. J. Phys. Oceanogr. 33, 1365–1379.
Yousif, R., Warren, C., Ben-Hamadou, R., Husrevoglu, S., 2018. Modeling sediment transport in Qatar: Application for coastal development planning. Integr. Environ. Assess. Manag. 14, 240–251.
Yu, Y., Notaro, M., Kalashnikova, O.V., Garay, M.J., 2016. Climatology of summer Shamal wind in the Middle East. J. Geophys. Res. Atmos. 121, 289–305.